Journal Pre-proofs

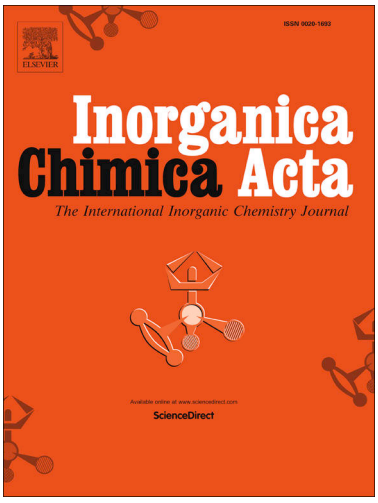

Research paper

Exploring the therapeutic potential of Cu(II)-complexes with ligands derived from pyridoxal

Patrique Nunes, Fernanda Marques, Isabel Cavaco, João Costa Pessoa, Isabel Correia

PII: S0020-1693(19)31677-9
DOI: https://doi.org/10.1016/j.ica.2020.119558
Reference: ICA 119558

To appear in: *Inorganica Chimica Acta*

Received Date: 4 November 2019
Revised Date: 22 January 2020
Accepted Date: 26 February 2020

Please cite this article as: P. Nunes, F. Marques, I. Cavaco, J. Costa Pessoa, I. Correia, Exploring the therapeutic potential of Cu(II)-complexes with ligands derived from pyridoxal, *Inorganica Chimica Acta* (2020), doi: https://doi.org/10.1016/j.ica.2020.119558

Exploring the therapeutic potential of Cu(II)-complexes with ligands derived from pyridoxal

Patrique Nunes,[a] Fernanda Marques,[b] Isabel Cavaco,[a,c] João Costa Pessoa,[a] Isabel Correia[a,*]

[a] *Centro de Química Estrutural, Departamento de Engenharia Química, Instituto Superior Técnico, Universidade de Lisboa, Av. Rovisco Pais, 1049-001 Lisboa, Portugal.*

[b] *Centro de Ciências e Tecnologias Nucleares, Instituto Superior Técnico, Universidade de Lisboa, Estrada Nacional 10, 2695-066 Bobadela LRS, Portugal.*

[c] *Departamento de Química Bioquímica e Farmácia, Universidade do Algarve, Campus de Gambelas, 8005-139 Faro, Portugal*

*To whom correspondence should be addressed:

Isabel Correia

e-mail: icorreia@tecnico.ulisboa.pt

Tel: +351 218 419 270

Fax: +351 218 419 239

Abstract

Three new copper(II) complexes formulated as [Cu(L)(X)], where X= H_2O or Cl and H_2L is a Schiff base ($H_2L^{1,2}$) or its reduced version (H_3L^3Cl) derived from pyridoxal, are prepared, as well as two ternary complexes [Cu(L)(phen)] also containing 1,10-phenanthroline. All compounds are characterized by the usual techniques: elemental analyses, ESI mass spectrometry, UV-Vis absorption, FTIR and EPR spectroscopies. The ligands coordinate the Cu(II) center forming complexes with square-planar based geometries. Their antioxidant properties are evaluated with a radical scavenging activity assay, with one of the ligand precursors showing activity higher than the positive control, ascorbic acid. The antiproliferative activity of all compounds is evaluated against two cancer cell lines: ovarian (A2780) and breast (MCF7). All complexes show moderate to excellent activity with the ternary Cu-complexes showing IC_{50} values between 0.7-9.3 μM after 24 h of incubation, values much lower than those reported for cisplatin, the reference drug. The hydrolytic stability of the complexes and their ability to bind albumin and DNA are evaluated by spectroscopic techniques, showing that the compounds bind bovine serum albumin. The [Cu(L)(phen)] complexes show ability to target DNA via intercalation.

Keywords: Pyridoxal, Schiff bases, copper, cytotoxicity, albumin

1. Introduction

Cancer is a health problem with very high impact in modern society and cancer deaths are estimated to rise as life expectancy increases; therefore, the interest in developing new anticancer metallodrugs with higher efficacy and presenting less adverse side effects is a growing research area.

Vitamin B_6 comprises a group of compounds that are involved in a multiplicity of biochemical reactions. Most of these reactions are co-catalyzed by the B_6 vitamer, pyridoxal-5'-phosphate, making it a crucial and versatile co-factor in numerous cell-metabolic processes [1, 2]. Additionally, vitamin B_6 is an antioxidant and incubation of cancer cells with high doses of pyridoxal or pyridoxine yielded significant reduction in cell proliferation when compared to control cultures [3]. Interest in metal coordination of B_6-vitamers started with the discovery of non-enzymatic model-systems containing pyridoxal and metal ions that could mimic enzymatic reactions involving vitamin B_6, by formation of Schiff base (SB) complexes [1]. Our group has worked extensively on the speciation and therapeutic potential of metal complexes derived from pyridoxal Schiff bases and reduced Schiff bases [4-8]. The V(IV) and Zn(II) complexes of these ligands exhibited antidiabetic activity [4, 9]. Also, one of the V(IV)-SB complexes previously reported by us [5], showed selective cytotoxicity for human melanoma and lung carcinoma cells, with a mechanism involving apoptosis triggered by increase in reactive oxygen species (ROS) formation [10].

Pyridoxal isonicotinoyl hydrazone derivatives and its iron complexes have shown anti-neoplastic activity and/or protection against oxidative stress [11-13]. Pyridoxal thiosemicarbazone Cu(II) complexes showed suppressive effect on erythroleukemia proliferation [14] and Co(III) complexes exhibited significant activity against breast (MCF7) and cervix (HeLa) cancer cells [15]. Therefore, exploration of pyridoxal-containing complexes has high potential to successfully develop effective chemotherapeutics.

Copper complexes are gaining importance as alternative anticancer drugs, anticipating that their endogenous character may induce less systemic toxic side effects [16-18]. Additionally, the use of aromatic N-heterocycles as co-ligands in the metal ion coordination could allow targeting DNA, as this type of molecules have shown high ability to bind to DNA double strands [19-23]. Inspired by these findings,

copper(II) complexes were prepared containing ligands derived from vitamin B_6 vitamers, as well as ternary complexes also containing 1,10-phenanthroline. In this report, we describe the synthesis, characterization and biological assessment of these new Cu(II) complexes. The compounds were characterized in solution and in the solid state and their stability and ability to bind albumin and DNA were evaluated. Their cytotoxicity was determined in two human tumoral cell lines and the influence of different structural elements on the biological performance of the compounds is discussed.

2. Experimental

2.1. Materials and methods

Pyridoxamine dihydrochloride and pyridoxal hydrochloride were purchased from Merck, 2-aminophenol from Reidel-de-Haen, salicylaldeyde from Acros, sodium borohydride from Alfa Aesar and DPPH from Sigma-Aldrich. All chemicals were p.a. grade and used without further purification, unless otherwise stated. The ^{1}H and ^{13}C NMR spectra were obtained on Bruker Avance+ 400 MHz and 300 MHz spectrometers. ^{1}H chemical shifts (δ) are expressed in ppm relative to the deuterated solvent residual peak. Electronic absorption spectra (UV-Vis) were recorded with a Perkin Elmer Lambda 35 spectrophotometer. Circular Dichroism (CD) spectra were recorded at 25 °C on a Jasco J-720 spectropolarimeter with an UV–Vis (180–800 nm) photomultiplier (EXEL-308). Infrared spectra (IR, 4000–400 cm^{-1}) were recorded either on a Nicolet Impact 400D or a BIO-RAD FTS 3000 MX spectrophotometers in KBr pellets; wavenumbers are expressed in cm^{-1}. Elemental analyses were carried out at Laboratório de Análises of Instituto Superior Técnico, using an FISONS EA 1108 CHNS-O apparatus. A LCQ Fleet™ Ion Trap Mass Spectrometer from Thermo Scientific was used to measure ESI-MS spectra of methanolic solutions of the complexes for characterization, and of aqueous solutions (3% DMSO-NH_4HCO_3 aqueous buffer, pH 7.4) for stability evaluation. A DIONEX ICS-1500 ion chromatography system, equipped with an IonPac® AS14A 4-mm analytical (4×250 mm) column and a suppressed conductivity at 10 µSFS ASRS®-ULTRA AutoSuppression® recycle mode detection system was used for chloride determination. Fluorescence measurements were carried out on a SPEX® Fluorolog

spectrofluorometer (Horiba Jobin Yvon) in a FL3-11 configuration, equipped with a Xenon lamp. The instrumental response was corrected by means of a correction function provided by the manufacturer. The experiments were carried out at room temperature and are all steady-state measurements.

2.2. Synthesis

4-(((2-hydroxybenzylidene)amino)methyl)-5-(hydroxymethyl)-2-methylpyridin-3-ol (H_2L^1)

H_2L^1 was prepared by adding a solution of pyridoxamine dihydrochloride (0.482 g, 2.00 mmol) to 10 mL of methanol with KOH at pH *ca.* 9.0. After 30 minutes the white solid (KCl) was filtered off and salicylaldehyde (0.213 mL, 2.00 mmol) dissolved in 6.5 mL of methanol:$CHCl_3$ (8% v/v) was added to the solution. The reaction mixture was refluxed at 50 ºC for 3 h, under stirring. After cooling the pH was adjusted to *ca.* 7.0 with methanolic HCl and the reaction volume was reduced under vacuum till precipitation occurred. The mixture was kept at 4 ºC overnight and the yellow solid that formed was filtered, washed with water, cold methanol and diethyl ether and dried under vacuum. Yield: 91%, 0.412 g. MM ($C_{15}H_{16}N_2O_3$) = 272.3 g/mol. Elemental Analysis**:** Calc. for $C_{15}H_{16}N_2O_3.0.5H_2O$: C, 64.04; H, 6.09; N, 9.96; Found: C, 63.8; H, 6.1; N, 9.9. ESI-MS: *m/z* [Found (Calcd)]: 271.9 (271.3) (25%) $[L\text{-}H]^-$; 543.2 (543.6) (100%) $[2L\text{-}H]^-$; 273.13 (273.3) (100%) $[L+H]^+$. UV-Vis in DMSO, λ_{max}/nm ($\varepsilon/M^{-1}cm^{-1}$): 285 (7965), 315 (3782), 413 (183); ^{1}H NMR (dmso-d_6, δ/ppm): 2.38 (s, 3H, H^{19}); 4.55 (s, 2H, H^{16}); 4.88 (s, 2H, H^9); 6.82-6.89 (m, 2H, H^2 and H^6); 7.30 (t, 1H, H^1); 7.43 (d, 1H, H^3); 7.96 (s, 1H, H^{12}); 8.61 (s, 1H, H^7); 5.20 (s, 1H, R-OH); 9.05 (s, 1H, Ar-OH) and 13.30 (s, 1H, Ar-OH). ^{13}C NMR (dmso-d_6, δ/ppm): 19.87 (C^{19}); 52.33 (C^9); 58.95 (C^{16}); 116.53 (C^6); 118.53 (C^2); 118.76 (C^4); 130.20 (C^{11}); 131.54 (C^3); 132.40 (C^1); 134.11 (C^{10}); 139.68 (C^{12}); 146.23 (C^{14}); 149.46 (C^{15}); 160.51 (C^5) and 166.14 (C^7). LogP = 1.29 [24].

5-(hydroxymethyl)-4-(((2-hydroxyphenyl)imino)methyl)-2-methylpyridin-3-ol (H_2L^2)

H_2L^2 was prepared by stirring 2-aminophenol (0.218 g, 2.00 mmol) dissolved in 6 mL of methanol/KOH pH *ca.* 9.0 and pyridoxal hydrochloride (0.407 g, 2.00 mmol) in 8 mL methanol, at room temperature for 3 h. After cooling the mixture was kept at 4 ºC overnight and the orange solid was filtered, washed with water, cold methanol and diethyl ether and dried under vacuum. Yield: 85%, 0.390 g. MM ($C_{14}H_{14}N_2O_3$) =

258.3 g/mol. Elemental Analysis**:** Calc. for $C_{14}H_{14}N_2O_3$: C, 65.11; H, 5.46; N, 10.85; Found: C, 64.9; H, 5.7; N, 10.7. ESI-MS: *m/z* [Found (Calcd)]: 259.15 (259.3) (100%) $[L+H]^+$; 257.11 (257.29) (100%) $[L-H]^-$. UV-Vis in dmso, λ_{max}/nm ($\varepsilon/M^{-1}cm^{-1}$): 295 (8282), 360 (11601), 463 (421); ^{1}H NMR (dmso-d_6, δ/ppm): 2.55 (s, 3H, H^{17}); 4.89 (s, 2H, H^{18}); 6.97 (t, 1H, H^2); 7.07 (d, 1H, H^6); 7.28 (t, 1H, H^1); 7.69 (d, 1H, H^3); 7.98 (s, 1H, H^{12}); 9.30 (s, 1H, H^9); 5.63 (s, 1H, R-OH) and 10.45 (s, 1H, Ar-OH). ^{13}C NMR (dmso-d_6, δ/ppm): 16.15 (C^{17}); 57.83 (C^{18}); 116.82 (C^6); 119.64 (C^2); 119.73 (C^3); 121.82 (C^{11}); 129.43 (C^{12}); 130.45 (C^1); 131.30 (C^4); 136.82 (C^{10}); 147.13 (C^{14}); 151.98 (C^{15}); 156.28 (C^9) and 157.82 (C^5). LogP = 2.21 [24]

5-(hydroxymethyl)-4-(((2-hydroxyphenyl)amino)methyl)-2-methylpyridin-3-ol (H_3L^3Cl)

H_3L^3Cl was obtained by reducing H_2L^2 (0.250 g, 0.970 mmol) with an excess of $NaBH_4$ in the presence of KOH in MeOH at room temperature for 48 h. A beige colored solid was obtained, washed with water and diethyl ether and dried under vacuum. Yield: 40%, 0.100 g. MM ($C_{14}H_{17}Cl_2NaN_2O_3$) = 355.1 g/mol. Elemental Analysis**:** Calc. for $C_{14}H_{17}N_2O_3NaCl_2.2.5H_2O$: C, 42.02; H, 5.54; N, 7.00; Cl, 17.72. Found: C, 42.2; H, 5.4; N, 6.8, Cl, 18.0. ESI MS: *m/z* [Found (Calcd)]: 259.61 (259.11) (10%) $[L-H]^-$; 295.17 (295.1) (100%) $[L+Cl]^-$; 297.02 (297.07) (25%) $[L+K-2H]^-$. UV Vis in dmso, λ_{max}/nm ($\varepsilon/M^{-1}cm^{-1}$): 285 (744), 342 (159); ^{1}H NMR (D_2O, δ/ppm): 2.67 (s, 3H, H^{17}); 4.64 (s, 2H, H^{18}); 4.79 (s, 2H, H^9); 6.89 (t, 1H, H^2); 6.97 (d, 1H, H^6); 7.23-7.29 (m, 2H, H^1 and H^3) and 8.17 (s, 1H, H^{12}). ^{13}C NMR (D_2O, δ/ppm): 15.4 (C^{17}); 45.03 (C^9); 58.49 (C^{18}); 116.86 (C^6); 120.74 (C^2); 121.42 (C^4); 123.89 (C^3); 130.95 (C^{12}); 131.55 (C^1); 134.06 (C^{10}); 138.90 (C^{11}); 142.46 (C^{14}); 149.62 (C^5) and 153.63 (C^{15}). LogP = 1.10 [24]

General synthesis of the [Cu(L)(X)] complexes (X = H_2O or Cl)

Copper(II) complexes **1**-**3** were obtained by drop-wise addition of 1 mL of $CuCl_2$ (1.00 mmol) in methanol to a stirred solution of 7-10 mL of a methanolic solution of the appropriate ligand precursor (1.00 mmol), followed by addition of a few drops of KOH in methanol to adjust the pH at *ca.* 7.5-8.0. The mixture was stirred at room temperature for ~4 h and kept in the fridge overnight. The solids formed were separated by filtration, washed with water, a small amount of cold methanol or acetone and diethyl ether, and dried under vacuum.

*K[Cu(L^1)Cl] (**1**)* - A dark green solid was obtained. Yield: 24%, 0.042 g. Elemental Analysis**:** Calc. [$C_{15}H_{14}N_2O_3ClCu$]K•0.5H_2O: C, 43.16; H, 3.62; N, 6.71; Cl, 8.49; Found: C, 43.1; H, 3.4; N, 6.5; Cl, 8.9. ESI-MS**:** *m/z* [Found (Calcd)]: 368.04 (368.00) (20%) $[M+Cl]^-$; 378.2 (378.0) (57%) $[M+FA-H]^-$; considering M the neutral complex without chloride and potassium ions; FA is formic acid. UV-Vis in dmso, λ_{max}/nm ($\varepsilon/M^{-1}cm^{-1}$): 266 (11447), 320 (4718), 370 (3498) and 670 (113). EPR parameters (DMSO, 3mM): $g_\perp$ = 2.071, $g_{||}$ = 2.280, $A_\perp$ = 16.5×10^{-4} cm^{-1} and $A_{||}$ = 180.7×10^{-4} cm^{-1}; (MeOH, 3mM): $g_\perp$ = 2.058, $g_{||}$ = 2.278, $A_\perp$ = 16.8×10^{-4} cm^{-1} and $A_{||}$ = 176.9×10^{-4} cm^{-1}

[Cu(L^2)(H_2O)] (**2**) - A dark red solid was obtained. Yield: 66%, 0.210 g. MM ($C_{14}H_{14}N_2O_4Cu$) = 337.8 g/mol. Elemental Analysis**:** Calc. for $C_{14}H_{14}CuN_2O_4$: C, 49.78; H, 4.18; N, 8.29; Found: C, 49.5; H, 3.7; N, 8.1. ESI-MS**:** *m/z* [Found (Calcd)]: 179.74 (178.48) (45%) $[M+H+K]^{2+}$, 397.77 (398.09) (10%) $[M+H_2O+IsoProp+H]^+$, 364.38 (364.0) (100%) $[M+FA-H]^-$, 683.35 (683.0) (60%) $[2M+FA-H]^-$, considering M the neutral complex without H_2O. UV-Vis in DMSO, λ_{max}/nm (ε/M^{-1} cm^{-1}): 281 (10251), 420 (9391, sh) and 457 (10818).

Na[Cu(L^3)Cl] (**3**) - A dark red solid was obtained. Yield: 57%, 0.062 g. Elemental Analysis**:** Calc. for [$C_{14}H_{14}N_2O_3ClCu$]Na•0.5H_2O: C, 43.21; H, 3.88; N, 7.20; Cl, 9.11; Found: C, 43.5; H, 3.4; N, 7.0; Cl, 9.5. ESI-MS [Found (Calcd)]: 356.54 (356.00) (90%) $[M+Cl]^-$, 366.41 (366.03) (90%) $[M+FA-H]^-$, 397.82 (397.95) (100%) $[M+2K-H]^+$, considering M the neutral complex without the chloride and sodium ions. UV-Vis in DMSO, λ_{max}/nm ($\varepsilon/M^{-1}cm^{-1}$): 286 (11540), 422 (8804), 454 (10282).

General synthesis of the complexes [Cu(L)(phen)]

Copper(II) complexes **4** and **5** were prepared by drop-wise addition of 1 mL of $CuCl_2$ (1.00 mmol) in methanol to a stirred solution of 7-10 mL of a methanolic solution of the appropriate ligand precursor (1.00 mmol), followed by the addition of few drops of KOH in methanol to adjust the pH at *ca.* 7.5-8.0. The mixture was stirred at room temperature for 15 min and 1,10-phenanthroline (1.00 mmol) was added drop wise. The mixture was stirred for another 4 h and kept in the fridge overnight. The resulting solid was filtrated and washed with water, cold ethanol or methanol and diethyl ether, dried under vacuum and recrystallized from methanol, when necessary.

*[Cu(L^1)(phen)] (**4**)* - A green solid was obtained. Yield: 66%, 0.210 g. MM ($C_{27}H_{22}CuN_4O_3$) = 514.07 g/mol. Elemental Analysis**:** Calc. [$C_{27}H_{22}CuN_4O_3$]•0.5H_2O:

C, 62.00; H, 4.43; N, 10.71; Found: C, 62.1; H, 4.2; N, 10.7. ESI-MS: *m/z* [Found (Calcd)]: 514.02 (514.1) (100%) $[M+H]^+$, 178.72 (179.37) (23%) $[M+2H+Na]^{3+}$. UV-Vis in dmso, λ_{max}/nm ($\varepsilon/M^{-1}cm^{-1}$): 275 (49367), 293 (21402), 371 (4833), 450 (744) and 672 (159). EPR parameters (MeOH, 3mM): $g_\perp = 2.080$, $g_{||} = 2.268$, $A_\perp = 36.9\times10^{-4}$ cm^{-1} and $A_{||} = 167.9\times10^{-4}$ cm^{-1}

*[Cu(HL^2)(phen)]Cl (**5**)* - An orange solid was obtained. Yield: 55 %, 0.136 g; MM ($C_{26}H_{20}N_4O_3Cu$) = 500.02 g/mol. Elemental Analysis: Calc. for $[C_{26}H_{21}N_4O_3ClCu]\bullet1.5H_2O$: C, 55.42; H, 4.29; N, 9.94; Found: C, 55.8; H, 4.2; N, 9.8. ESI-MS: *m/z* [Found (Calcd)]: 500.08 (499.97) (75%) $[M+H]^+$; 999.16 (1000.4) (28%) $[2M+H]^+$; 498.07 (497.27) (45%) $[M-H]^-$, considering M the neutral complex without the Cl^- ion and not protonated. UV-Vis in dmso, λ_{max}/nm ($\varepsilon/M^{-1}cm^{-1}$): 295 (17357), 400 (6811) and 467 (6620). EPR parameters (DMF, 3mM): $g_\perp = 2.058$, $g_{||} = 2.247$, $A_\perp = 32.0\times10^{-4}$ cm^{-1} and $A_{||} = 181.0\times10^{-4}$ cm^{-1}; (MeOH, 3mM): $g_\perp = 2.077$, $g_{||} = 2.278$, $A_\perp = 46.6\times10^{-4}$ cm^{-1} and $A_{||} = 160.8\times10^{-4}$ cm^{-1}

2.3. Chloride determination by anion exchange chromatography

The compounds were stirred overnight at room temperature in an aqueous solution containing 0.1 - 1.0 M of H_2SO_4, with a minimum amount of DMSO (used to dissolve the complexes), to obtain a final concentration of *ca.* 4 mM. The resulting solutions were diluted with Milli-Q water in order to obtain Cl^- concentrations within the calibration curve. The calibration curve was determined by preparing a concentrated stock solution of 500 ppm of Cl^- ion in Milli-Q water. This stock solution was diluted to obtain five solutions of Cl^- with concentrations ranging from 5.0 to 50 ppm. The solutions of the samples were injected and the Cl^- concentration determined.

2.4. Evaluation of the radical scavenging activity

Stock solutions (2.0 mM) of the compounds were diluted to obtain concentrations of 9.0, 19, 28, 37 and 74 μM in methanol. To each solution 1.25 mL of DPPH (2,2-diphenyl-1-picrylhydrazyl, 50 μM) in methanol was added and the final volume (3.5 mL) was obtained by adding methanol. The solutions were kept in the dark for 30 min. The radical scavenging activity (RSA) [25] was evaluated by following the decrease of DPPH absorbance at 517 nm. The data were collected between 300-

700 nm, and the values were converted into percentage of RSA, according to the following formula:

$$\%RSA = \frac{(Abs_{standart} - Abs_{sample}) \times 100}{Abs_{standart}} \quad (1)$$

where Abs_{sample} is the absorption of DPPH solutions containing the test compound and $Abs_{standart}$ is the absorption of DPPH in methanol. All ligands and complexes have negligible absorbance under the applied concentrations at 517 nm (thus, no interference between absorption of the tested compounds and DPPH). Ascorbic acid was chosen as the positive control.

2.5. Cytotoxicity assays

The cytotoxicity of the complexes was evaluated by the MTT assay (MTT = 3-(4,5-dimethylthiazol-2-yl)-2,5-diphenyltetrazolium bromide) against A2780 ovarian and MCF7 breast cancer cells in 96-well plates (2-3x10^6 cells/well). The compounds were first dissolved in DMSO to prepare a 10 mM stock solution and then in medium through serial dilutions in the range 0.1-100 µM. The final DMSO concentration was 1% (v/v) for the highest complex concentration; this amount showed no cytotoxic effect. After treatment with the complexes, the cell medium was replaced by 200 µL of a MTT solution in PBS (0.5 mg/mL) and further incubated for 24 h at 37 °C. The resulting purple formazan crystals from the tetrazolium reduction were dissolved in 200 µL DMSO. The absorbance of controls and cell-treated wells was measured at 575 nm using a microplate reader (PowerWave Xs, Biotek Instruments, USA). The cytotoxicity of the complexes was expressed as the IC_{50} values calculated from dose-response curves using the GraphPad Prism software (vs. 5.0).

2.6 Stability studies

2.6.1. UV-Vis

Stability studies were performed in organic and aqueous medium by measuring absorption spectra with increasing time. Stock solutions of complexes and ligands were prepared in DMSO with concentrations ranging from 0.5 to 1.0 mM. Sample solutions were prepared by dilution of the stock solutions in DMSO, NH_4HCO_3 (25 mM, pH~7.4) or PBS (10 mM, pH = 7.4, 2.7mM KCl and 0.137 M NaCl), to obtain

final concentrations between 23 and 143 μM, with <5% DMSO (v/v) in the aqueous solution samples.

2.6.2. ^{1}H NMR

The stability of ligand precursors H_2L^1, H_2L^2 and H_3L^3Cl were monitored at room temperature and at various time intervals for up to 24 h by ^{1}H NMR spectroscopy. Solutions of each ligand (*ca.* 20 mM) were prepared in DMSO-d_6 and diluted in either DMSO-d_6 or D_2O containing PBS buffer (10 mM, pH=7.4) to obtain final concentrationd of *ca.* 1.0 mM.

2.7. BSA binding studies

The binding of metal complexes to BSA (bovine serum albumin) was evaluated by UV-Visible and Circular Dichroism (CD) spectral measurements. Stock solutions of BSA were obtained by dissolving the protein in PBS buffer (10 mM, pH~7.4), which was kept at 4 ºC for at least 3 h to fully hydrate. The albumin concentration was determined by measuring the absorbance at 279 nm, considering the molar extinction coefficient 44309 $M^{-1}cm^{-1}$ [26]. Concentrated stock solutions of Cu^{II}-complexes were prepared in DMSO and diluted with PBS buffer, due to their limited solubility in aqueous media; the amount of DMSO in the samples was less than 5 %.

2.7.1. UV-Vis

Electronic absorption spectroscopy was used for monitoring (up to 24 h) the compounds stability and also interactions with BSA. Samples containing BSA (*ca.* 25 μM) and each complex in 1:1 molar ratio (<5 % DMSO v/v) were prepared. All spectra were recorded in 10 mm optical path quartz cells (240-700 nm). The same amount of BSA was added to the reference cell to cancel the contribution from the albumin spectrum.

2.7.2. Circular dichroism

BSA solution in PBS buffer (*ca.* 385 μM) was titrated with *ca.* 3.4 mM of **1** or **2** dissolved in DMSO to obtain Cu(II)/BSA molar ratios ranging from 0.02 to 0.5 (<5 % DMSO). The CD spectra of the solutions were measured and after reaching the Cu(II)/BSA = 0.5 molar ratio for **1** or 0.2 molar ratio for **2**, the CD spectra of the solutions were periodically recorded up to 22 h. Blank assays were measured for

each CD spectrum with the same concentration of both complexes and DMSO without the protein.

2.7.3. Fluorescence

Successive additions of stock solutions of the complexes in DMSO were directly introduced into the cuvette containing BSA (*ca.* 0.68 μM) in HEPES buffer (pH 7.4, 10 mM) to obtain a Cu(II)/BSA molar ratios ranging from 0.3 to 22 (<4% v/v DMSO). The fluorescence emission spectrum was recorded for each ratio between 303 and 550 nm using the following parameters: λ_{ex} = 295 nm, excitation and emission slit band-widths of 5.0 nm. Blank assays were measured for each sample. The data were corrected for absorption and inner-filter-effects.[27, 28]

The fluorescence quenching data were plotted according to the Stern-Volmer equation [29]:

$$\frac{I_0}{I} = 1 + K_{SV}[Q] \qquad (2)$$

where I_0 and I are the relative fluorescence intensities of the BSA protein in the absence and presence of the quencher, respectively. [*Q*] is the quencher concentration and K_{sv} is the Stern-Volmer quenching constant.

The K_{SV} constants were obtained from the linear regression of the plot of $\frac{I_0}{I}$ *vs.* [Q]. The binding constants were determined using the Scatchard equation [30]:

$$\frac{\Delta I / I_0}{[Q]} = nK_{Sch} - K_{Sch}\frac{\Delta I}{I_0} \qquad (3)$$

where K_{sch} represents the binding constant obtained from the slope of the plot of $\frac{\Delta I / I_0}{[Q]}$ *vs* $\frac{\Delta I}{I_0}$ and n is the number of binding sites per protein molecule.

2.8. DNA binding

2.8.1. ctDNA solutions preparation

Stock solutions of *calf thymus* DNA (*ct*DNA) were prepared by dissolving the solid in PBS buffer (10 mM, pH=7.4), and kept at 4 ºC for at least 48 h for hydration. The absorbance ratio (A_{260}/A_{280}) of *ca.* 1.9 indicated that the *ct*DNA was sufficiently

protein-free. The *ct*DNA stock solutions concentration was calculated based on their absorbance at 260 nm, using the per nucleotide extinction coefficient ε_{260} = 6600 M^{-1} cm^{-1} [31].

2.8.2. Electronic absorbance spectroscopy

Successive aliquots of *ct*DNA stock solution (ca. 3 mM) in PBS were added to solutions of the complexes (15.9-35.5 μM) in PBS (< 2.5% DMSO, v/v) to obtain final concentrations of *ct*DNA ranging from 2.3 – 111 μM. The mixtures were equilibrated for 5 min prior to UV-Vis spectroscopy measurements. To compensate the contribution of *ct*DNA and DMSO absorption exactly equal amounts of *ct*DNA and DMSO were added to the sample and reference cells in each measurement (250-600 nm). 10 mm optical path length quartz cells were used. Based on the UV-Vis absorption variation the binding constants were determined by fitting the data to the Kaminoh equation [32].

$$\mathbf{Abs} = \frac{\mathbf{A_0 + K[DNA]A_{Sat}}}{\mathbf{1 + K[DNA]}} \quad (4)$$

Where A_{Sat} is the absorbance value under saturation conditions, A_0 is the absorbance of the complex alone; K is the Kaminoh constant determined from the plot of Abs *vs.* [*ct*DNA].

The binding constants (K_{BC}) of the complex to *ct*DNA were also determined by fitting the data with the Scatchard equation [33]:

$$\frac{[ctDNA]}{\Delta\varepsilon_{ap}} = \frac{[ctDNA]}{\Delta\varepsilon} + \frac{1}{\Delta\varepsilon K_{BC}} \quad (5)$$

where $\Delta\varepsilon_{ap} = [\varepsilon_a - \varepsilon_f]$; $\Delta\varepsilon = [\varepsilon_b - \varepsilon_f]$; ε_a is the ratio between the absorption measured and the complex concentration (Abs/[complex]); ε_b and ε_f is the extinction coefficient of the compound bound to *ct*DNA and free in solution, respectively; [*ct*DNA] is concentration of *ct*DNA (in base pairs) and K_{BC} is the intrinsic binding constant calculated by the representation of [*ct*DNA]/$\Delta\varepsilon_{ap}$ *vs.* [*ct*DNA].

2.8.3. Circular Dichroism

Circular dichroism titrations of **4** and **5**, which contain phenanthroline as co-ligand, with *ct*DNA were done keeping the concentration of *ct*DNA constant while varying the complexes' concentration. *ct*DNA solutions were titrated by adding small amounts of the complexes dissolved in DMSO (1.0-1.9 mM) to obtain complex/DNA molar ratios ranging from 0.02 to 1.5. The assays were performed directly in the 10 mm quartz cuvette and the CD spectra were collected from 230 to 600 nm with 1 nm bandwidth using a UV photomultiplier. Blank spectra were measured without *ct*DNA and subtracted from the corresponding sample.

3. Results and discussion

3.1. Synthesis and characterization

Schiff base ligands H_2L^1 and H_2L^2 were obtained in good yields by condensation between either pyridoxamine and salicylaldehyde or pyridoxal and 2-aminophenol (see Scheme 1). The reduced Schiff base H_3L^3Cl was obtained in moderate yield (40%) by reduction of H_2L^2 with $NaBH_4$. All compounds were characterized by elemental analysis and the usual spectroscopic techniques [see Experimental part and Supplementary Material (SM) for details], which confirmed the proposed formulations.

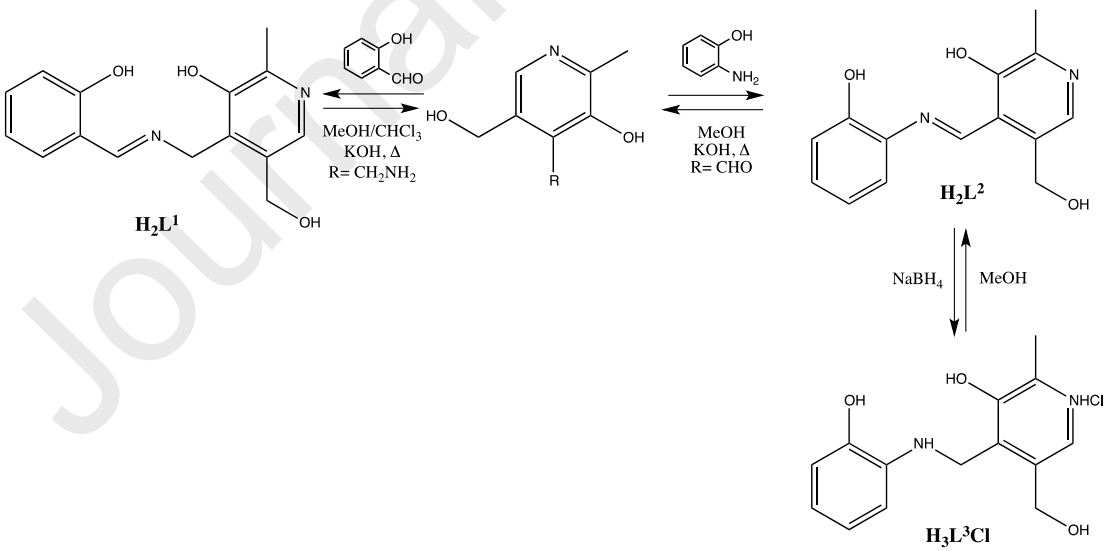

Scheme 1. Reaction scheme for the synthesis of the Schiff bases (H_2L^{1-2}) and reduced Schiff base (H_3L^3Cl).

The ligand precursors reacted with $CuCl_2$ in methanol, yielding Cu(II)-complexes **1**-**3**, in moderate yields. In the reactions in which phenanthroline was also added, ternary [Cu(L)(phen)] complexes (**4** and **5**) were obtained also in moderate yields. All complexes are new and were characterized in the solid state and in solution by the usual spectroscopic techniques, which will be discussed in detail in the following sections. The formulation proposed for the complexes is depicted in Figure 1.

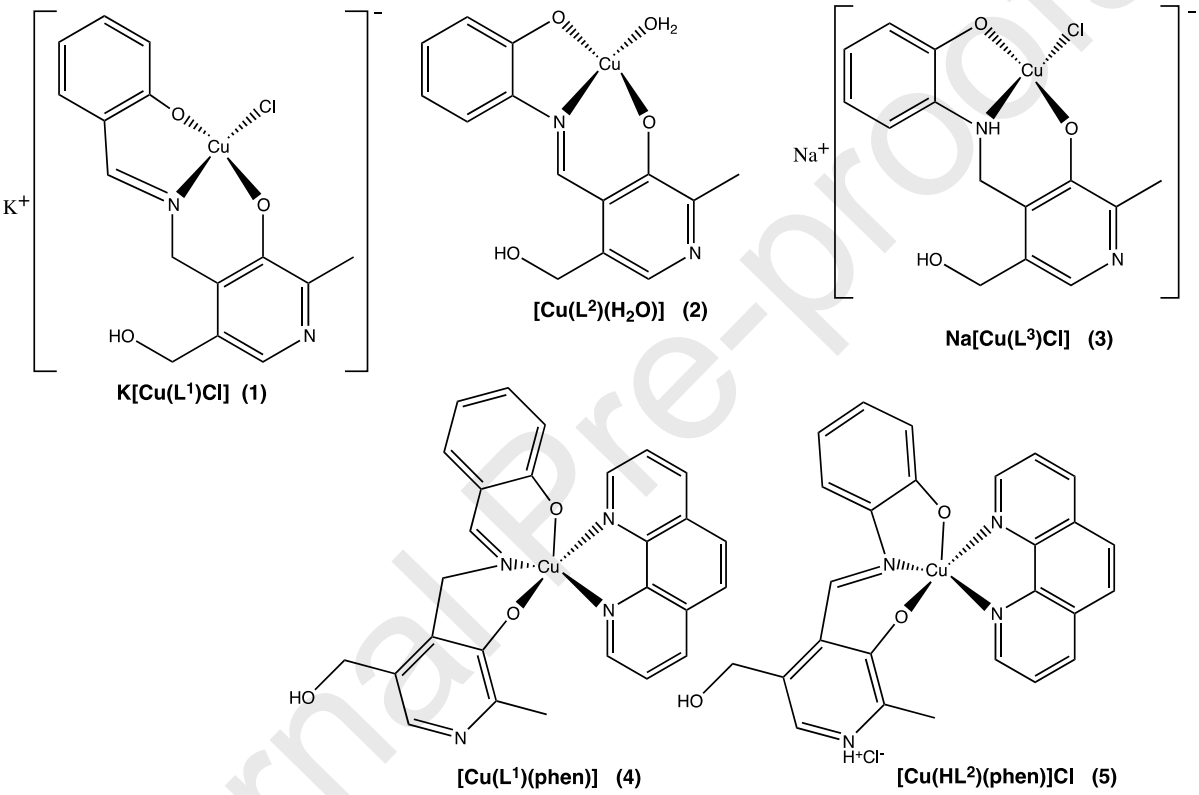

Fig. 1. Molecular formulas proposed for the prepared Cu^{II} complexes.

All compounds were characterized by ESI-MS spectrometry and the spectra are collected in SM (see also the Experimental part). In most cases it was possible to identify the molecular ion peaks in the positive, $[L+H]^+$ or $[M+H]^+$, or negative mode, $[L-H]^-$ or $[M-H]^-$, as well as the copper isotropic pattern in the complexes' peaks. Adducts with formic acid or isopropanol were also found in the MS spectra of some metal complexes. The presence of chloride ions in complexes and ligands was confirmed by anion exchange chromatography. For complexes **1**, **3** and **5,** only one chloride ion was detected, while two were determined for H_3L^3Cl. For the remaining

complexes and ligand precursors it was not possible to carry out the chloride determination due to their low solubility, and thus, formulations were proposed based on elemental analysis and mass spectrometry data.

3.1.1 NMR spectroscopy

The 1D and 2D ^{1}H NMR and ^{13}C NMR spectra of the ligands were measured at room temperature in DMSO-d_6 or D_2O (Table 1). The azomethine proton signal for H_2L^1 appears as a singlet at 8.61 while for H_2L^2 this proton is much more deshielded appearing at 9.30 ppm. However, the corresponding azomethine carbon is more shielded in H_2L^1 than in H_2L^2, possibly due to additional conjugation with the aromatic system of the pyridoxal moiety in H_2L^2. For H_3L^3Cl the azomethine proton signal is not detected, as expected. Also, the appearance of a signal at 4.79 ppm, attributed to a CH_2 moiety, resulting from the azomethine reduction, was difficult to distinguish in the ^{1}H NMR spectrum due to overlap with the proton signal of residual water. However, this signal was undoubtedly identified in the HSCQ NMR experiment (see Fig S1.1.17), which showed a cross peak at 4.79 ppm (^{1}H NMR) and 45.03 ppm (^{13}C NMR). The broad signals observed downfield for the samples dissolved in DMSO-d_6 (H_2L^1 and H_2L^2) correspond to the hydroxyl protons. These exchangeable protons were identified by its disappearance after addition of small amounts of D_2O (data not shown). For H_2L^1 the two deshielded signals (~ 13.30 and 9.05 ppm) are assigned to the aromatic hydroxyl protons, while the peak at 5.20 ppm is assigned to the aliphatic hydroxyl proton. However, for H_2L^2 the resonances of the exchangeable protons disappear after the addition of a drop of D_2O, followed by hydrolysis (see section 3.4). The chemical shift of all protons and carbons are listed in Experimental section and the respective spectra are collected in SM.

Table 1

Selected peaks and assignment for protons and carbon atoms of the NMR spectra (chemical shift / ppm).

Compound / solvent		CH=N	CH_2N	CH_{pyr}	CH_3	$H_{aromatic}$
H_2L^1 / DMSO-d_6	^1H	8.61	-	7.96	2.38	6.82-7.45
	^{13}C	166.14	-	139.68	19.87	116.53-149.46
H_2L^2 / DMSO-d_6	^1H	9.30	-	7.98	2.55	6.95-7.71
	^{13}C	156.28	-	129.43	16.15	116.82-151.98
H_3L^3Cl / D_2O	^1H	-	4.79	8.17	2.67	6.86-7.29
	^{13}C	-	45.03	130.95	15.42	116.86-153.63

3.1.2 FTIR

Selected IR bands of the prepared compounds are collected in Table 2. Assignments were made based on the literature [34] and by comparison of the spectra of complexes and respective ligand precursors to determine groups involved in coordination, as shifts and/or intensity changes are expected to occur upon coordination of the ligand to the metal ion.

All compounds present broad bands in the region between 2700-3500 cm^{-1}, corresponding to absorption bands of the OH groups involved in hydrogen bonding (symmetrical and asymmetrical) and overtone N-H bands. The IR spectra of the Schiff base ligands show the characteristic strong ν(C=N) band at 1643 and 1597 cm^{-1}, for H_2L^1 and H_2L^2, respectively (Fig S1.1.21). In the complexes' spectra, the ν(C=N) absorption appears at slightly lower energy indicating coordination to the copper(II) ion. A similar behavior was observed for the bands assigned to the ν(C-O)$_{phenolate}$ (*ca.* 1250 cm^{-1}), which is compatible with the involvement of this group in the coordination to the Cu(II) ion [35]. The phenolic O-H stretching vibration is observed in the free ligands between 3140 and 3427 cm^{-1}. Upon complexation the disappearance of the O-H stretching absorption is expected, due to the deprotonation and coordination to the metal center. Nevertheless, the presence of the aliphatic O-H group from the pyridoxal moiety, together with the presence of water molecules in the complexes adds some difficulty to establish by FTIR the

coordination of ligands by the phenolic donor group to the metal center. On the other hand, the two absorption bands at 3220 and 3376 cm^{-1} of the reduced Schiff base ligand (H_3L^3Cl) may originate from the vibration of the asymmetrical and symmetrical stretching modes of the ν(N-H) group [36]. At 3429 cm^{-1} (appearing as a shoulder) the band might be attributed to ν(OH) vibrations. Moreover, the H_3L^3Cl ligand precursor presents two weak bands around 2700 and 2600 cm^{-1} associated with the amine salt functional group of the reduced Schiff base [34], which corroborates the proposed formulation. These peaks disappear when the ligand is coordinated to the Cu(II) center.

Table 2

Selected FTIR bands and assignments for the ligand precursors and Cu(II) complexes (cm^{-1}).

Compound	ν(O–H)	ν(C=N) imine	ν(N-H)	ν(C-O) phenolate	ν(C-O) alcohol
H_2L^1	3422 3142	1642	---	1246	1035 1023
H_2L^2	3362	1597	---	1236	1032 1010
H_3L^3Cl	3429	---	3376 3220	1279	1039 1020
1	3340	1628	---	1241	1040
2	3341 3218	1587	---	1201	1049 1019
3	3429 3350	---	---	1260	1047 1017
4	3428 3164	1635	---	1243	1031
5	3447 3277	1583	---	1206	1040 1014

3.1.3. Electronic absorption spectra

The UV-Vis spectroscopic characterization was done in DMSO by measuring spectra at different concentrations (see SM). Figure 2 shows the spectra measured for all compounds. For the Schiff bases H_2L^{1-2}, a strong band is observed between 315 and 360 nm, which can be assigned to the n→π* transition, associated with the azomethine bond. This band is not detected in the spectrum of the reduced Schiff base H_3L^3Cl and the molar absorptivity is much higher for H_2L^2 than H_2L^1. Probably this difference is due to the extended conjugated π system that is present in H_2L^2, since the transition dipolar moment is higher in π-conjugated systems and consequently the transition probability increases [37]. Closer observation shows that this band is rather broad in H_2L^2 and must be, in fact, two bands: the n→π* and π→π*□□□□□□□ due to the extended conjugation system suffer strong bathochromic shifts, when compared to their position in H_2L^1. Bands centered at *ca.* 285 nm, present in the spectra of all compounds are due to π→π* intraligand transitions. Complexes **4** and **5** show very strong bands in the UV region due to the presence of the aromatic N-heterocyclic 1,10-phenanthroline ligand. The spectra of the Cu-complexes show the presence of ligand to metal charge transfer (LMCT) bands at *ca.* 450 nm, due to transitions from the phenolate to the metal center. Bands in the visible were observed for solutions of complexes **1** and **4** at *ca*. 670 nm (see Fig S1.2.2 and S.1.2.11) due to d-d transitions [38, 39]. Although present in the spectra of the other Cu-complexes they are not easily observed.

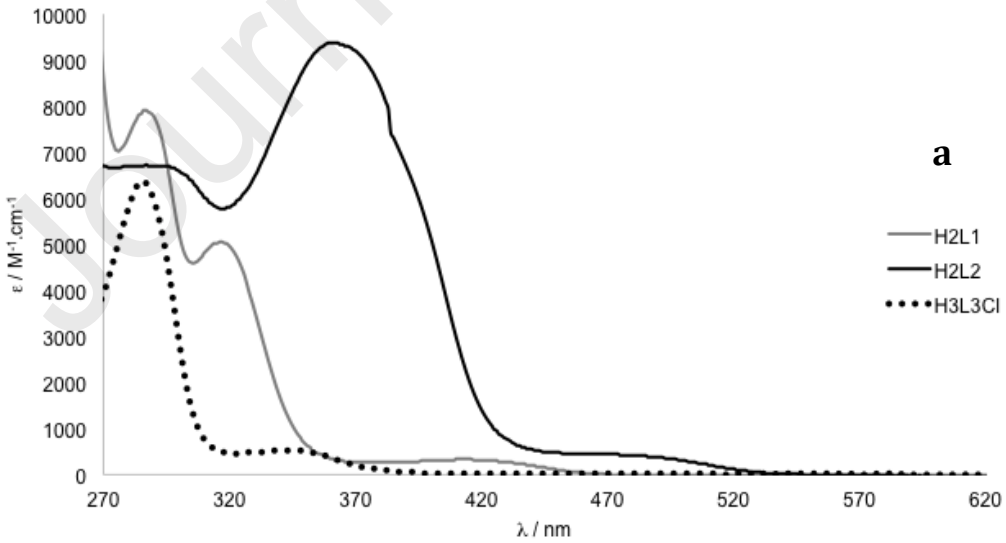

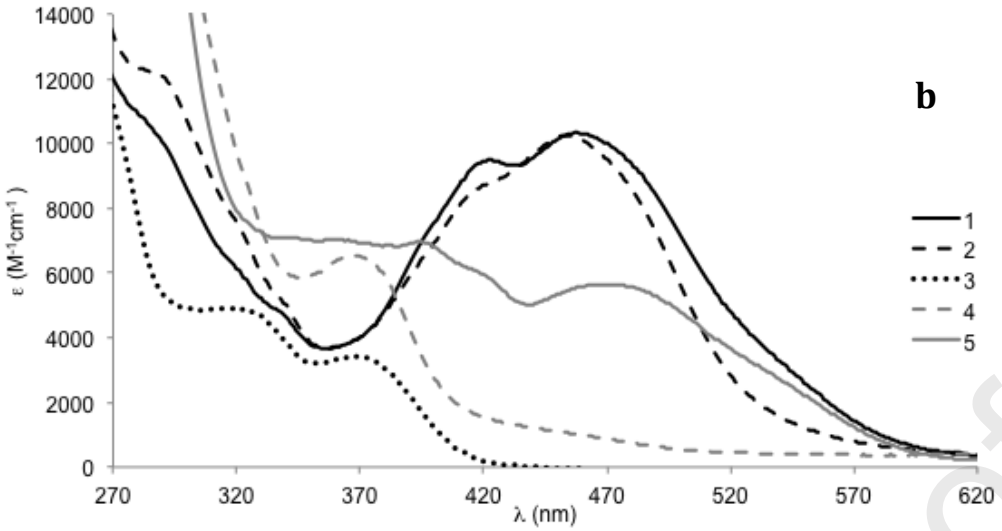

Fig. 2. Electronic absorption spectra of ligand precursors (a) and complexes (b) measured in DMSO.

3.1.4. Electronic Paramagnetic Resonance

The X-band EPR spectra of the Cu(II) complexes were recorded at 77 K or 100K. ~~Complexes **1-4** were dissolved~~ in DMSO, DMF or MeOH ~~and complex **5** in DMF.~~ All complexes show spectra with axial symmetry and $g_{||} > g_{\perp} > 2.0$, indicating the presence of a dx^2-y^2 ground state with copper(II) located in square-based geometries, but only **1, 4** and **5** show well resolved spectra with four hyperfine coupling bands in the high field region. No super hyperfine coupling was observed in any complex spectra. Figure 3 shows the spectrum measured for complex **1** in DMSO and the one obtained by simulation [40] which yielded the spin Hamiltonian parameters included in Table 3. The empirical ratio g_z/A_z calculated for complexes **1, 4** and **5** is ~~134 and 130 cm, respectively,~~ within the interval 100 - 135 cm, which according to Addison *et. al.* [41] indicates the presence of small distortions in square-based coordination geometries. The remaining complexes (**2** and **3** ~~and **4**~~**)** display broad bands and poor resolution spectra with g~2.1 (Fig. S1.2.16). This can be ~~due~~ attributed to lower solubility but it is probably due to ~~or~~ formation of ~~aggregates and~~ oligomeric species. It is reasonable to assume that the molecular geometry of complexes **1**, **2** and **3** are square planar, while complexes **4** and **5** assume a pyramidal square-based geometry which is in agreement with similar structures proposed for related compounds.[42-45]

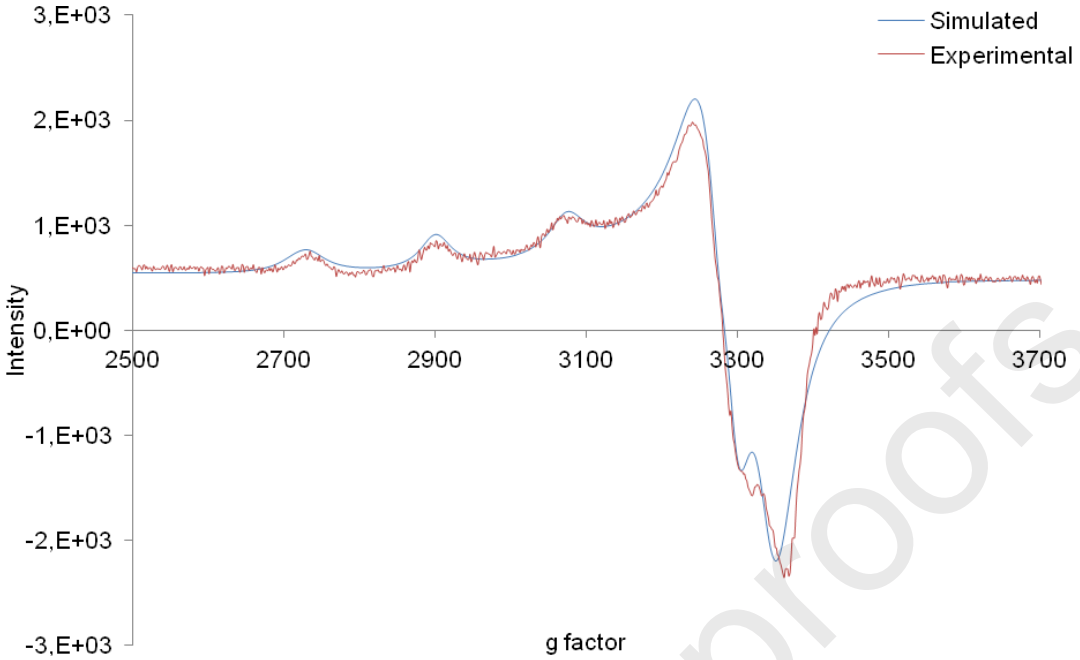

Fig. 3. First derivative X-band EPR spectrum measured for **1** in DMSO (*ca.* 3 mM) as well as the simulated spectrum, which yielded the parameters listed in Table 3.

Table 3

EPR spin Hamiltonian parameters of Cu(II) complexes **1**, **4** and **5**.

Complex	Solvent	$g_{\|\|}$	$g_{\perp}$	$A_{\|\|}$(x10^4 cm^{-1})	$A_{\perp}$(x10^4 cm^{-1})	$g_{\|\|}/A_{\|\|}$ (cm)
1	DMSO	2.280	2.071	180.7	16.5	134
1	MeOH	2.278	2.058	176.9	16.8	129
4	MeOH	2.268	2.080	167.9	36.9	135
5	DMF	2.247	2.058	181.0	32.0	130

3.2. Radical scavenging activity

~~1,1-Diphenyl-2-picryl-hydrazyl (~~DPPH~~)~~ is a stable free radical that has one delocalized unpaired electron. The radical forms deep purple coloured solutions in organic solvents, which upon reaction with other radicals, electrons, or hydrogen atoms, leads to the formation of a colourless species. Following the absorbance at 517 nm of solutions prepared with different ratios of compound/DPPH allows the assessment of their radical scavenging activity. Therefore, the DPPH assay was

used to evaluate the antioxidant potential of the complexes and their respective ligand precursors (see experimental part). Correlations have been found for the radical scavenging activity and redox potentials of compounds [46-48]. Table 4 shows the effective concentration (IC_{50}) obtained for all compounds. Complexes **1**, **4** and **5** show similar and moderate activity, bellow 100 μM. Unexpectedly, H_2L^2 shows very high radical scavenging capacity, ~~even better than~~ comparable to the positive control, ascorbic acid. However, reduction of the C=N bond (in H_3L^3Cl) resulted in total loss of the radical scavenging activity. While for H_2L^1 coordination to Cu(II) increases considerably its activity (compare IC_{50} values for H_2L^1 and **4**) for H_2L^2 and H_3L^3Cl this did not happen, as both corresponding Cu-compounds show very poor antioxidant activity. Complexes **4** and **5,** containing phen, show equal or higher antioxidant potential than **1** and **2**, which do not have the aromatic N-base.

The very high radical scavenging activity observed for H_2L^2 is probably related to its extended conjugated system, which stabilizes the phenolic radical, which is formed upon transfer of a hydrogen atom from its hydroxyl group.

Table 4

IC_{50} values (μM) of the scavenging activity determined for the synthetized compounds by the DPPH assay. The standard deviation of 3 replicates is included.

Compound	IC_{50} /μM
H_2L^1	704 ± 172
H_2L^2	14 ± 4
H_3L^3Cl	417 ± 36
1	83 ± 4
2	172 ± 26
3	443 ± 17
4	85 ± 14
5	83 ± 11
Ascorbic acid	11.6

3.3 Cytotoxicity assays

The cytotoxic activity of the complexes and ligand precursors (Table 5) was evaluated on ovarian (A2780) and breast (MCF7) human cancer cell lines, after 24 h

of incubation. The IC_{50} values were determined using the MTT assay, which measures the mitochondrial dehydrogenase activities in living cells.

All compounds exhibited moderate to very high *in vitro* cytotoxicity against both cancer cell lines (IC_{50} values ranging from 0.7 and 86 μM) while the ligand precursors are not active (IC_{50} > 100 μM), at least within the time frame chosen, 24 h. Comparison between the two different cell types showed that compounds containing the phen ligand exhibit higher cytotoxicity against the ovarian cancer cells than the breast cells, while the other complexes showed more efficacy against the breast cells. The complex containing the reduced Schiff base (**3**) revealed lower activity than the ~~other~~ one with the Schiff base (**2**) in both cell lines. Taking into account the similarity of the ligands and the lipophilicity of the compounds, H_2L^2 is expected to be much more lipophilic than H_3L^3Cl, the logP order being H_2L^2 > H_2L^1 > H_3L^3Cl [24], and thus, a similar order is expected for their copper complexes. Therefore, for **2** and **3** lipophilicity can be correlated with cytotoxicity. However, other properties must also be at play since IC_{50} (**1**) > IC_{50} (**3**) and LogP (**1**) > LogP (**3**).

Most complexes are comparable to, or much better than cisplatin, which showed moderate activity for these cells at 24 h incubation. For both tumor cells the ternary complexes containing phen showed IC_{50} values much lower than cisplatin. Overall, data shows that there is a relevant enhancement of the anti-proliferative activity due to the synergetic effect of combining Cu(II) and a Schiff base, which is further enhanced by the presence of phen coordinated to the metal center, increasing significantly the cytotoxicity, particularly in the ovarian cancer cell line, with a decrease in IC_{50} of more than 30 times.

Table 5

Cytotoxicity (IC_{50} in μM ± SD) of the ligand precursors and copper(II) complexes on two human cancer cells (A2780 and MCF7) after 24 h of incubation.

Compound	A2780	MCF7
1	86 ± 38	34 ± 11
2	23 ± 8.5	6.8 ± 3.5
3	49 ± 18	19 ± 5.7
4	1.8 ± 0.6	9.3 ± 3.0
5	0.7 ± 0.1	2.6 ± 1.0
phen, H_2L^1, H_2L^2 and H_3L^3Cl	>100	>100
$[Cu(phen)_2]$	0.4 ± 0.2	1.5 ± 0.4
cisplatin [49]	36 ± 8.0	59 ± 12

3.4 Stability studies

The stability of the Schiff bases $H_2L^{1,2}$ was evaluated in aqueous buffer by ^{1}H NMR and UV-Vis absorption spectroscopy, as this type of ligand typically hydrolyzes in the presence of water containing solvents. The studies shown in SM confirm that the Schiff bases $H_2L^{1,2}$ indeed hydrolyze in the presence of water. The same assays were carried out for the reduced Schiff base H_3L^3Cl and, as expected,[50] no signs of hydrolysis were observed (Fig. S3.4).

The stability of the complexes in organic solvents was followed by UV-visible spectroscopy in DMSO. All Cu(II)-complexes are stable, maintaining their original spectra with minor changes after *ca.* 24 h (Fig. S3.7a-S3.11a). In order to mimic physiological conditions, the stability was also evaluated in pH 7.4 buffered media (PBS or NH_4HCO_3) containing a minimum amount of organic solvent. The behavior of the compounds in aqueous solvent over time is very similar for both buffer solutions. Complexes **2** and **3** start to precipitate after 30 minutes at concentrations ≥ 25 μM. The same solubility issue occurs for **5** (after 2 h), with lower absorbance values being recorded with time, but no evident changes in the absorption bands' position. Complex **1** is stable for at least 24 h and **4** shows only very small spectral changes over time (less than 10 % of absorbance decrease at λ = 356 nm after 24 h) (Fig. S3.10b). The small changes observed in most spectra may simply be due to solvent exchange (H_2O and DMSO).

As general conclusion, the Schiff base ligands suffer hydrolysis in aqueous solution under conditions mimicking physiological media, although when coordinated to Cu(II) their stability increases considerably. The complexes maintain their structure during the time frame usually necessary to carry out interactions studies with biomolecules.

3.5 Interaction with BSA

Serum albumins are the most abundant proteins in the blood vascular system. Human serum albumin (HSA) is *ca.* 60 % in the plasma and it is mainly involved in transport to cells [51]. It is widely accepted that the binding strength between a drug and albumin may influence its ADME (absorption, distribution, metabolism, and excretion) properties, which may lead to loss or enhancement of the drug's efficacy [52, 53]. In the following studies, BSA was chosen as model protein, due to its structural similarity to the homolog HSA [54] and to its relative importance in cell culture media assays, since it is present in relatively high concentrations. The cells ability to uptake the complexes may also depend on the binding strength between the compound and BSA or/and other complex species formed in solution that can have different affinities to this protein. Furthermore, several specific cell receptors for albumin have been reported in the literature [55], which may facilitate the complexes entry into cells. Therefore, understanding the interaction between this protein and the new complexes is extremely relevant to properly evaluate their therapeutic potential.

Besides one coordination position occupied by a labile molecule, complexes **1-3** have other coordinating positions that may be used to form ternary species of the type [Cu(L^n)(BSA)]. In complexes **4** and **5,** BSA coordination, if it occurs, may take place in the apical free position, with formation of an octahedral species, [Cu(L^n)(phen)(BSA)], or by loss of one of the ligands forming [Cu(L^n)(BSA)] or [Cu(phen)(BSA)] species. Other possibilities, for all complexes, is the loss of all ligands and binding as [Cu(BSA)] and [Cu_2(BSA)], since Cu(II) has high affinity for BSA with albumin paying an important role in copper transport in the bloodstream [56, 57]. Therefore, different spectroscopic studies were performed aiming to properly understand the binding of the complexes to BSA.

3.5.1. UV-visible spectra

Since the hydrolytic stability of the complexes may increase by binding to albumin, the stability of the complexes was evaluated in the presence of BSA, under the same experimental conditions used in its absence. In all cases, although no precipitation was observed by naked eye, the spectra measured for **2** and **3** show some evidences of precipitation, such as, lower absorbance intensity values recorded with time (Fig. S4.2 and S4.3).

For all complexes, changes were observed. For **1** (Fig. 4) it took *ca.* 1 h for the system to reach equilibrium; some bands shifted to lower energy, new bands appeared and isosbestic points were observed at 310, 340 and 395 nm. All these observations are consistent with the transformation of the original $[Cu(L^1)Cl]^-$ complex into a new species, possibly $[Cu(L^1)(BSA)]$. Comparison of the spectra (at t > 300 min, Fig. S4.1) of solutions containing BSA and either complex **1**, H_2L^1 or $[Cu^{2+} + H_2L^1]$ shows that it is quite difficult to see any differences between these spectra in the UV range, and therefore we cannot state without doubt that the observed time changes are due to formation of the ternary $[Cu(L^1)(BSA)]$ complex.

Complex **3** maintains the original UV-Visible spectrum in solution for at least 3 h, in the presence of BSA, with no signs of interaction, hydrolysis or precipitation, after which absorbance decreases (Fig. S4.3). Complex **4** shows a hyposochromic shift of ~3 nm of the band with maximum at 267 nm, after 24 hours, with two isosbestic points appearing at 337 and 383 nm, indicating that the complex interacts with BSA by forming a new species (Figure S4.4). Interestingly, there are quite a few similarities in the electronic absorption spectra obtained for complex **1** and **4** with time in the presence of 1 mole equivalent of BSA, such as the appearance of new bands around 320 and 410 nm. This probably indicates the formation of the same type of species, (*p.e.* $[Cu(L^1)(BSA)]$), although we cannot state it with certainty based only in UV-Vis experiments.

For complex **5** only minor changes are observed in the first 100 min, *p.e.* the band centered at 440 nm decreases its intensity and an isosbestic point is present at 336 nm. These are consistent with formation of a new species but the phen ligand should be in the coordination sphere of the metal ion as no changes are seen in the 267 nm band.

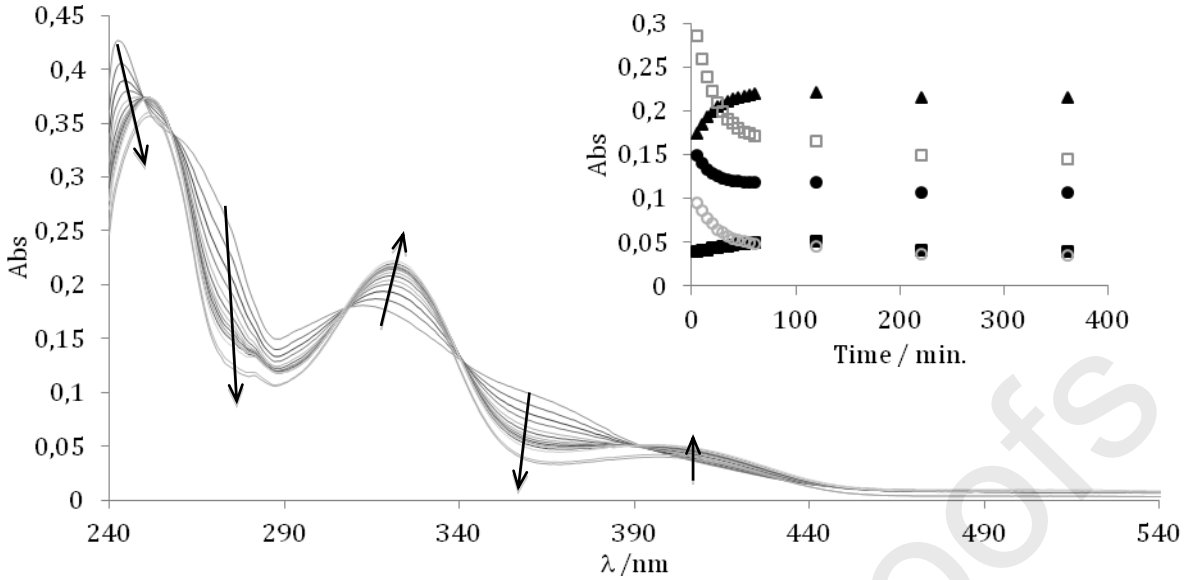

Fig. 4. Electronic absorbance of complex **1** (24.9 μM, 4.6 % DMSO v/v) with *ca.* 25 μM of BSA measured in PBS (10 mM, pH~7.4) with time. Inset: absorbance variation with time at λ = 403 nm (■); 363 nm (○); 321 nm (▲); 287 nm (●); 270 nm (□). The arrows show absorbance variations with time.

3.5.2. Circular dichroism

The prepared Cu(II)-complexes **1**-**3** are not chiral compounds (**3** and **4** may be considered racemic mixtures with chirality at the metal), and therefore their solutions do not show circular dichroism spectra. Upon binding to a chiral molecule, such as BSA, chirality transfer may happen between the biomolecule and the Cu-complex. Particularly interesting to observe are the copper d-d transitions as these may appear in the CD spectra and provide useful information concerning the coordination environment of the metal ion.

The CD spectra of BSA (388 μM) upon addition of increasing amounts of complex **1** are shown in Figure 5. Complex **1** is not optically active and BSA does not present absorption bands in the visible range studied, so, the induced CD (ICD) bands observed in Fig. 5 are clear proof of binding of the complex close to chiral groups of BSA. The positive band at *ca.* 490 nm and the negative band at *ca.* 560 nm somehow resemble the CD spectra of BSA when free Cu^{2+} is added (Fig. S4.10), however the presence of a new distinct negative band in this system at *ca.* 400 nm, confirms that this is a new species, probably [Cu(L^1)(BSA)]. At higher complex/BSA

molar ratios precipitation occurs, which precludes the observation of new Cu-BSA species for higher ratios. No relevant CD spectral changes were observed with time (up to 22 h) for a solution containing a complex/BSA molar ratio of *ca.* 0.5 (Fig S4.6). Very similar CD spectra, with the same shape and similar intensities were observed when complex **4** was added to BSA (Fig. S4.8-4.9), indicating that the formed BSA-**4** species probably shows the same type of binding, when compared with complex **1** and suggests that both CD-active species are analogous.

For complex **2** only a positive band at 420 nm developed upon addition of small amounts of the complex (see Fig. S4.7), however, precipitation for ratios higher than 0.2, did not allow performing a complete study.

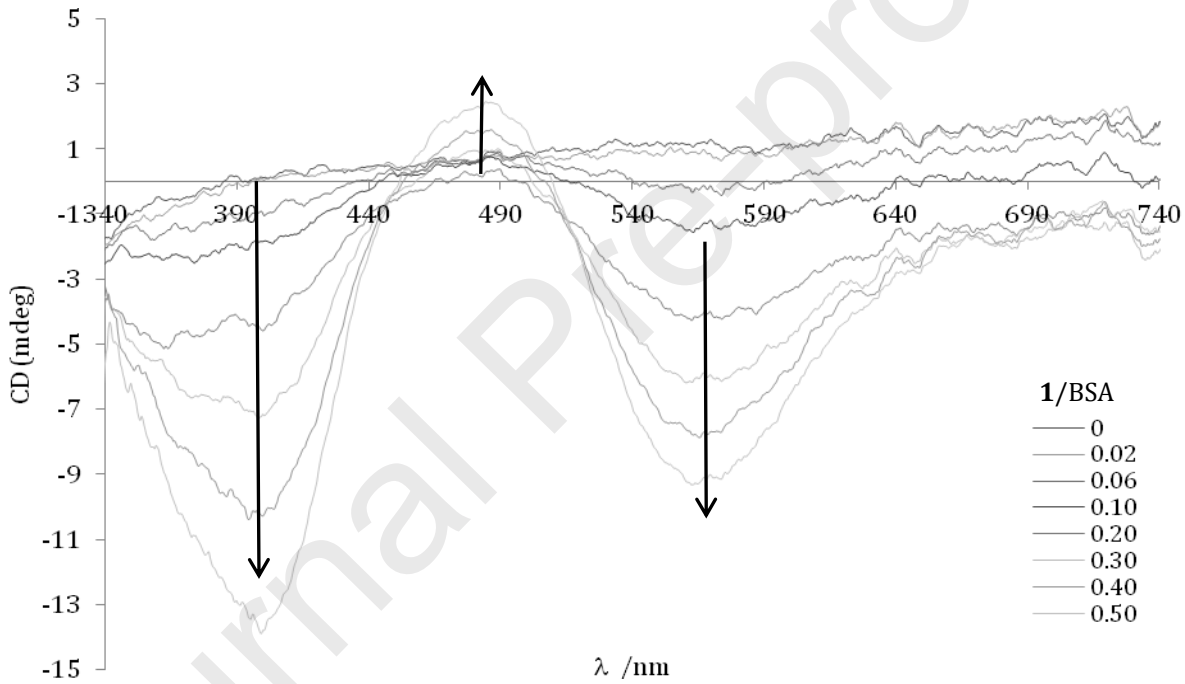

Fig. 5. CD spectra of a BSA titration (388 µM) with a solution of complex **1** (*ca.* 3.4 mM) in PBS buffer (pH 7.4, 10 mM, < 5 % DMSO). Complex **1**/BSA molar ratios are indicated in the figure.

3.5.3. Fluorescence

Fluorescence spectroscopy is one of the most commonly used techniques to evaluate the role of BSA in the transport of metallodrug candidates. BSA has intrinsic fluorescence due to the presence of fluorescent amino acids, the main contribution being related to two tryptophans located at positions 134 and 212 [58]. Trp-134 is on

the albumin surface in subdomain IB and Trp-212 is positioned within a hydrophobic pocket in subdomain IIA [54].

When BSA is excited at 295 nm, an emission band appears with maximum at *ca.* 340 nm. Under the same conditions complex **1** has intrinsic fluorescence and exhibits a band with a maximum centered at ca. 401 nm. Hence, the data obtained from the fluorescence quenching experiments were corrected by subtracting the spectra of the complex at each concentration. The emission intensity changes upon addition of complex **1** to BSA (Figure 6), this indicating a protein conformational change or binding between the protein and the complex, which may be covalent or by hydrophobic interactions (π–π stacking) [58]. Increasing the concentration of the metal complex leads to progressive quenching of the fluorescence intensity at 340 nm, up to 64%, simultaneous to the appearance of the complex emission at 401 nm, forming an isoemissive point at 379 nm. Additionally, a small blue shift of about 3 nm is observed. This energy change may indicate that the polarity at the binding site of the tryptophan environment in the protein decreases [59] indicating that the fluorescent residues become located in a more hydrophobic environment [60]. A similar blue shift in the fluorescence of BSA emission maximum is observed in the presence of the other Cu-complexes as well as for 2,4-dinitrophenol (DNP). For DNP binding to the protein was attributed to site I, in subdomain IIA [61].

Determination of binding constants is crucial for the development of a drug, since most of the drugs in the market can reversibly bind albumin with moderate affinity [binding constants in the range (1-15) × 10^4 M^{-1}] [62]. In the particular case of complex **1**, constants were calculated by applying the Stern-volmer (eq. 2) and Scatchard (eq. 3) models. A linear Stern-Volmer plot was obtained suggesting a single mechanism involving static quenching [63]. The binding constant shows that the binding between complex **1** and BSA is moderate: K_{SV} = 9.9 × 10^4 M^{-1} and K_{sch} = 9.2 × 10^4 M^{-1} (see SM). When comparing the binding strength between BSA and the complexes of the type [$Cu^{II}(L^n)$] no significant differences were found (Table 6). However, when the co-ligand phen is coordinated to the metal center, the binding affinity increases 3 to 4 times. It is known that the planarity of the ligands coordinating the metal center plays an important role in terms of the binding affinity to BSA [64] due to the importance of π–π stacking interactions with aromatic

residues. The higher binding strength of complexes **4** and **5** to albumin could be explained by the intrinsic planarity of the phen co-ligand.

Table 6

BSA binding constants obtained by fitting the fluorescence quenching data with the Scatchard (eq. 3) and Stern-Volmer (eq. 2) models.

	Scatchard	Stern-volmer
Complex	**K_{Sch} (× 10^4 M^{-1})**	**K_{SV} (× 10^4 M^{-1})**
1	9.3	9.9
2	9.7	7.9
3	8.1	8.0
4	37.1	13.5
5	30.2	34.1

Since BSA is one of the major components in the cellular medium used in cytotoxicity assays and knowing that, in blood, albumin is the second more important carrier of Cu(II) ions, these results indicate that a ~~reversible~~ complex/BSA adduct is formed and the compound is able to be stored/protected and carried by the protein.

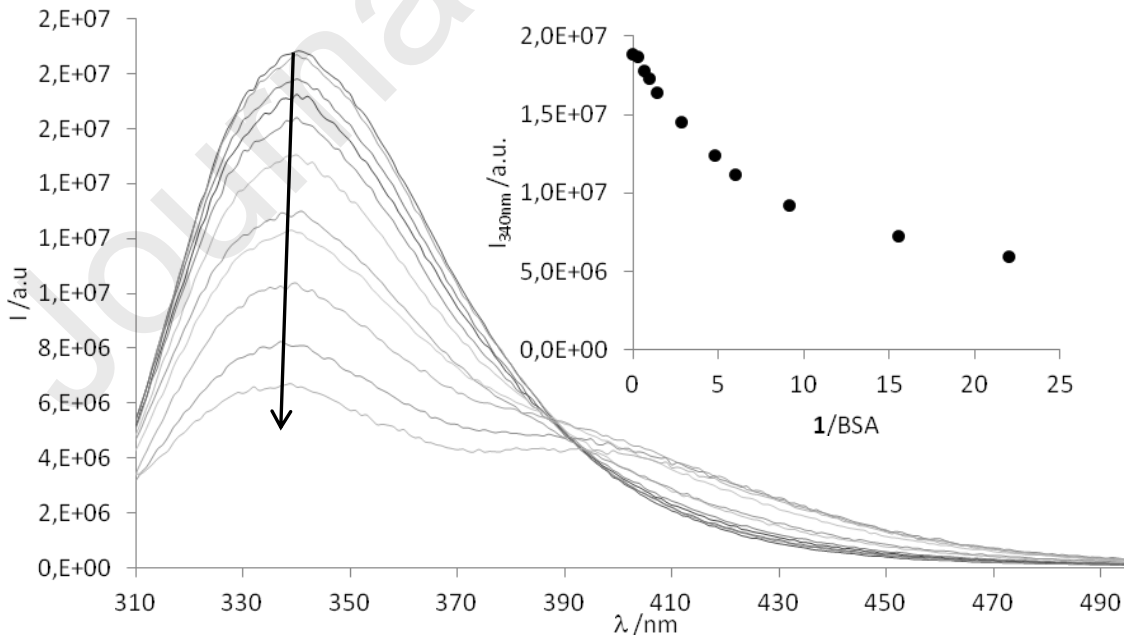

Fig. 6. Fluorescence emission spectra (λ_{ex} = 295 nm) of BSA (0.7 μM) with increasing concentrations of complex **1** (*ca*. 0.2-13.9 μM) in HEPES buffer (10 mM, pH 7.4) containing less than 4 % of DMSO (v/v). Inset: Plot of the λ_{em}^{max} = 340 nm *vs* **1**:BSA molar equivalents. The data were corrected for absorption and inner-filter-effects.

3.6 DNA binding studies

Evaluation of the interactions of the complexes and *calf thymus* DNA were performed using UV-Visible and CD spectrophotometric titrations.

3.6.1. CD spectroscopy

By taking advantage of the DNA chirality, relevant information about DNA structural changes can be obtained by CD spectroscopy, such as: conformation, possible cleavage and damage. The CD spectrum of *ct*DNA, which is in the right-handed B-form, shows a positive band (λ_{max} = 275 nm) corresponding to base stacking and a negative band centered at λ_{max} = 245 nm, attributed to right-handed helicity. We again highlight that the complexes under study do not display any CD spectra, meaning that any changes in the CD spectral titration will be related with the interaction of the studied complex with DNA.

A *ct*DNA solution in HEPES buffer was titrated with small aliquots of complexes **4** and **5** (~1 mM in DMSO) to obtain Cu(II)/*ct*DNA molar ratios ranging from 0.02 to 1. The resulting CD spectra were measured and are shown in Fig. 7. Spectral changes observed in both systems (of **4** and **5**) are similar, with two positive ICD bands appearing at λ_{max} = 279 and 300 nm (shoulder) after the first addition of the complex to *ct*DNA, followed by an intensity increase after subsequent additions. The increase is observed till complex/*ct*DNA molar ratios of *ca.* 0.5 and 1 for complex **4** and **5**, respectively. In the *ct*DNA negative band region (*ca.* λ_{max} = 245 nm) changes are not so evident, particularly when compared with the very strong positive ICD signal. The intensity increase indicates that complexes bind to *ct*DNA in such a way that the *ct*DNA helix expands. Similar results were obtained when titrating *ct*DNA with the co-ligand phen [65]. These changes are attributed to the intercalation of the aromatic phen rings in between the *ct*DNA base pairs. For **4** and **5** the $\Delta\varepsilon$ for a Cu(II)/DNA

ratio of 0.5 was *ca.* 6 and 12 $M^{-1}cm^{-1}$, respectively, while for phen it was also around 6 $M^{-1}cm^{-1}$. Thus, the *ct*DNA interaction with **5** (evaluation based solely on the intensity of the ICD bands) seems to be stronger.

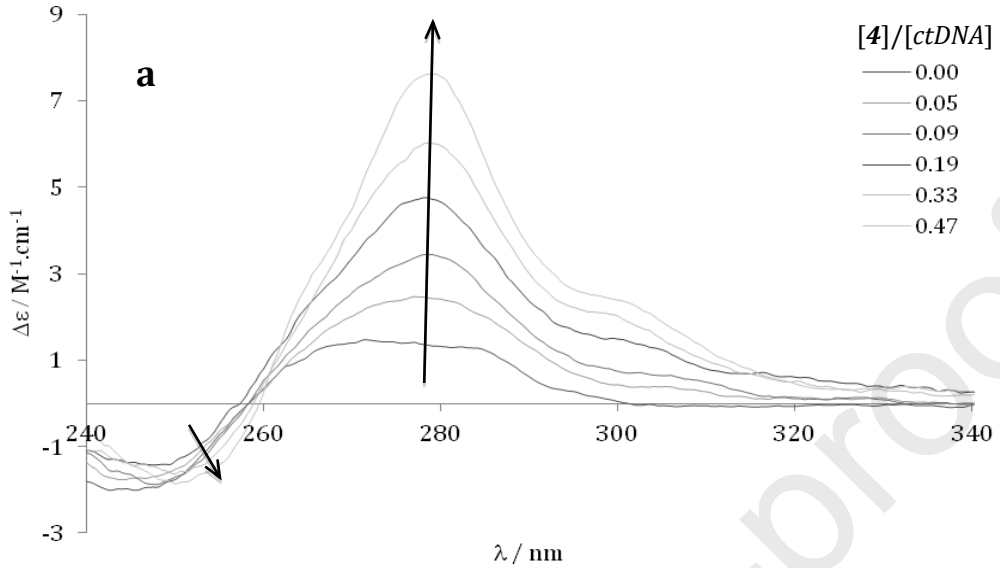

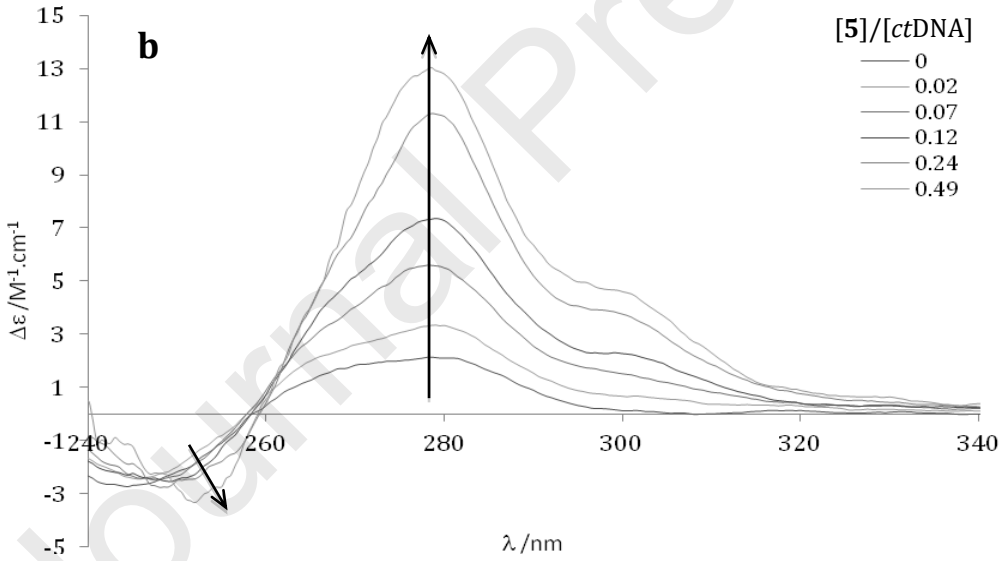

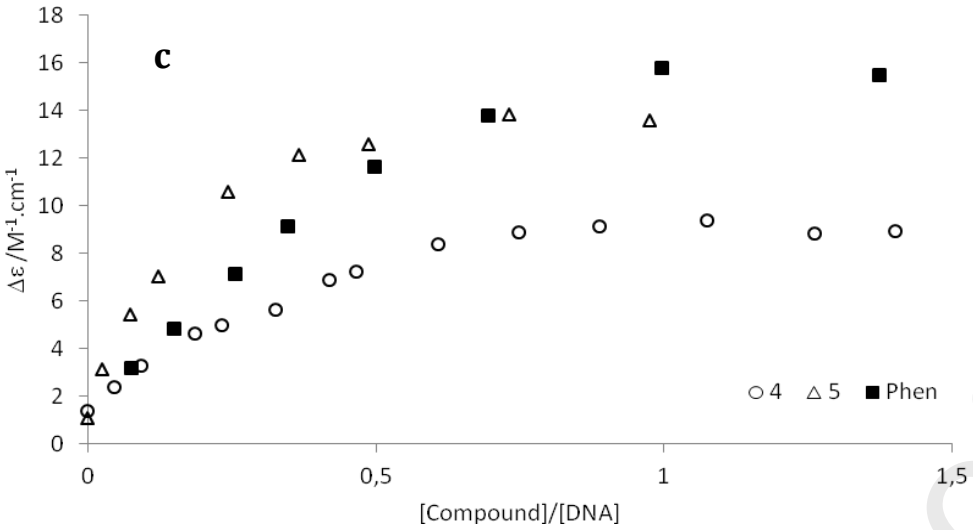

Fig. 7. Circular dichroism spectra (10 mm optical path) of *ct*DNA (76.6 μM) in HEPES buffer (10 mM, pH 7.4) with additions of a) complex **4** and b) complex **5**; c) variation of the $\Delta\varepsilon$ ($M^{-1}cm^{-1}$) with the molar ratio of compound: *ct*DNA for **4**, **5** and phen.

Additionally, comparison of the CD spectra of the systems containing **4** and **5** with the one reported by us for $[Zn(phen)_2]$ incubated with *ct*DNA [65] shows similarity in shape, intensity, and maxima, as well as the molar ratio after which no more changes are detected, suggesting that, most probably, the binding to *ct*DNA is driven by the phenanthroline co-ligand.

3.6.2. UV-Vis titrations

Since all complexes are stable for at least one hour in aqueous medium, titrations were also done by UV-Vis spectroscopy, which is a simple and adequate technique to study DNA binding. The same amount of *ct*DNA was added to both the sample and reference cells, and thus, changes are only due to interactions between complexes and DNA (see SM section S5). Fig. 8 shows the titration of complex **4** with *ct*DNA followed by UV-Vis absorption spectroscopy. The gradual decrease of the absorption intensity (hypochromism) at λ = 266, 290 and 360 nm, along with the increase in absorption intensity around 320 nm, as well as the presence of two isosbestic points at 300 and 341 nm are probably related with the phen co-ligand

moiety, since the complementary complex **1** does not show any absorption changes with the *ct*DNA addition (Fig. S5.1).

Complex **2** and **3** show similar behaviour when titrated with *ct*DNA (Fig. S5.2 and S5.3, respectively). Complex **3** titration presents hypochromism (5 nm of red shift at λ_{max} = 283 nm) while **2** presents a decrease of the absorption intensities associated with a red shift of 5 nm at λ_{max} = 283 nm and 7 nm at λ_{max} = 445 nm. Hypochromism and a red shift are usually associated with the intercalative binding mode of metal complexes to *ct*DNA, due to stacking interactions of the planar aromatic groups and the base pairs of *ct*DNA [66]. Thus, we can conclude that the changes observed are characteristic of intercalative binding of these complex to *ct*DNA.[67] The binding constant (K_{BC}) values included in Table 7 show similar *ct*DNA affinity for all complexes, with no particular differences between mixed-ligand complexes (containing phenanthroline co-ligand) and complexes of the type $Cu^{II}(L^n)$.

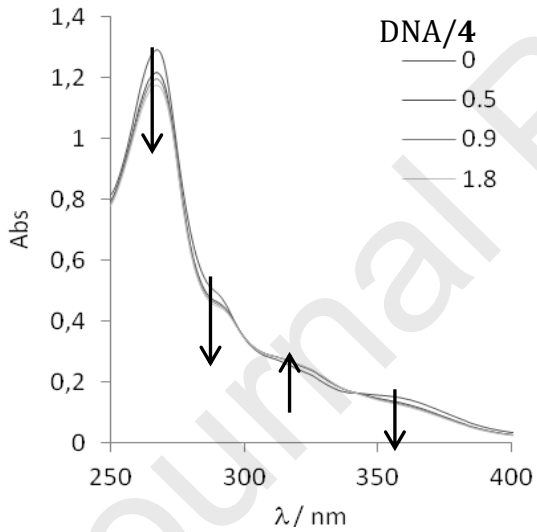

Fig. 8. Complex **4** titration (*ca.* 25 μM in PBS buffer, 25 mM, pH 7.4, 1.2 % of DMSO) with increasing amounts of *ct*DNA (3.3 mM in PBS buffer, 25 mM, pH 7.4). The *ct*DNA/**4** molar ratios are indicated.

Table 7

DNA binding constants (K_{BC}) obtained by fitting the UV-Visible titration data with the Scatchard (eq. 5) and Kaminoh (eq. 4) models.

	Scatchard	Kaminoh
Complex	**K_{BC} (x 10^5 M^{-1})**	**K_{BC} (x 10^5 M^{-1})**
1	No interaction	No interaction
2	2.2±0.7	4.2±0.8
3	1.5±0.3	1.7±0.6
4	1.4±0.2	1.5±03
5*	26±3.1	------

*meaningless binding constant value due to scattering observed immediately after the *ct*DNA addition.

4. Conclusions

Five new Cu-complexes, containing two Schiff bases and one reduced Schiff base derived from pyridoxal were synthesized in moderate yields and characterized by analytic and spectroscopic techniques. Spectroscopic studies showed that while the Schiff bases H_2L^1 and H_2L^2 are highly susceptible to hydrolysis in aqueous solvents, the reduced version H_3L^3Cl is much less prone to it, as well as the obtained Cu(II)-complexes, which are stable for at least 1 h. One of the ligand precursors, H_2L^2, but not its reduced version H_3L^3Cl, showed remarkably high radical scavenging activity, as evaluated by the DPPH assay, higher than the positive control, ascorbic acid.

The Cu(II) compounds correspond to either tetra- (**1**-**3**) or penta-coordinated (**4** and **5**) complexes in square-planar based geometries. H_2L^1 and H_2L^2 are quite similar in terms of donor atoms, forming tridentate ONO-chelates, however, H_2L^1 forms a (6+6)-chelate system while H_2L^2 forms a more strained (6+5)-chelate.

Regarding biological-related activity, complexes **2** and **5**, containing H_2L^2, showed higher antioxidant potential, higher cytotoxicity towards the two tested cancer cell lines and higher ability to bind *ct*DNA, when compared to **1** and **4**, respectively. Complex **2**, containing the Schiff base, shows lower antioxidant potential than **3** that involves its reduced version. Interestingly, complex **3** has higher antiproliferative activity, at least twice, than complex **2**. ~~Considering the similarity of the ligands, such differences may be explained by the lipophilicity of the compounds. H_2L^2 is expected to be much more lipophilic than H_2L^1, the logP order being H_2L^2 > H_2L^1 > H_3L^3Cl,[24]~~

~~and thus, a similar order is expected for their copper complexes.~~ Complexes **4** and **5** containing the heteroaromatic phenanthroline as co-ligand show similar moderate antioxidant activity (but higher than the observed for complexes **1**-**3**) and the best performance in terms of cytotoxicity, with IC_{50} values < 10 μM, and remarkably low against ovarian cancer cells for complex **5**: 0.7±0.1 μM. Noteworthy, this compound is the one that shows the highest ability to bind *ct*DNA.

Overall, the reported compounds show properties that make them interesting for further studies as potential anticancer drugs. Compound [Cu(L^2)(phen)], **5**, is the one that appears more promising, as it is stable, active, and able to target *ct*DNA. Its selectivity towards cancer cells and its mode of action require further evaluation to assert its potential.

Acknowledgments

This work was supported by *Fundação para a Ciência e a Tecnologia* (FCT) (project UID/QUI/00100/2019). Patrique Nunes acknowledges FCT for SFRH/BD/108743/2015 grant. The Portuguese NMR and Mass Spectrometry IST-UL Centers are acknowledged for the access to the equipment.

Supplementary Material

The following sections are included in the Supplementary data to this article:

S1 – Characterization of ligands and Cu-complexes

S2 – Radical scavenging activity

S3 – Stability studies

S4 – BSA binding studies

S5 – DNA binding studies

References

[1] A.E. Martell, Accounts Chem. Res., 22 (1989) 115-124.

[2] M. Parra, S. Stahl, H. Hellmann, Cells, 7(7) (2018) 84.

[3] T.D. Shultz, D. Lee, D.R. Stickney, D.S. Gridley, Nutr. Res., 9 (1989) 133-151.

[4] T. Mukherjee, J.C. Pessoa, A. Kumar, A.R. Sarkar, Dalton Trans., 41 (2012) 5260-5271.

[5] I. Correia, J.C. Pessoa, M.T. Duarte, R.T. Henriques, M.F.M. Piedade, L.F. Veiros, T. Jakusch, T. Kiss, A. Dornyei, M.M.C.A. Castro, C.F.G.C. Geraldes, F. Avecilla, Chem. Eur. J., 10 (2004) 2301-2317.
[6] I. Correia, J.C. Pessoa, M.T. Duarte, M.F.M. da Piedade, T. Jackush, T. Kiss, M.M.C.A. Castro, C.F.G.C. Geraldes, F. Avecilla, Eur. J. Inorg. Chem., (2005) 732-744.
[7] I. Correia, A. Dornyei, T. Jakusch, F. Avecilla, T. Kiss, J.C. Pessoa, Eur. J. Inorg. Chem., (2006) 2819-2830.
[8] I. Correia, A. Dornyei, F. Avecilla, T. Kiss, J.C. Pessoa, Eur. J. Inorg. Chem., (2006) 656-662.
[9] T. Mukherjee, J.C. Pessoa, A. Kumar, A.R. Sarkar, Inorg. Chem., 50 (2011) 4349-4361.
[10] M. Strianese, A. Basile, A. Mazzone, S. Morello, M.C. Turco, C. Pellecchia, J. Cell Physiol., 228 (2013) 2202-2209.
[11] J.L. Buss, J. Neuzil, N. Gellert, C. Weber, P. Ponka, Biochem. Pharmacol., 65 (2003) 161-172.
[12] J.L. Buss, B.T. Greene, J. Turner, F.M. Torti, S.V. Torti, Curr. Top. Med. Chem., 4 (2004) 1623-1635.
[13] P. Bendova, E. Mackova, P. Haskova, A. Vavrova, E. Jirkovsky, M. Sterba, O. Popelova, D.S. Kalinowski, P. Kovarikova, K. Vavrova, D.R. Richardson, T. Simunek, Chem. Res. Toxicol., 23 (2010) 1105-1114.
[14] M.B. Ferrari, G.G. Fava, P. Tarasconi, R. Albertini, S. Pinelli, R. Starcich, J. Inorg. Biochem., 53 (1994) 13-25.
[15] R. Manikandan, P. Vijayan, P. Anitha, G. Prakash, P. Viswanathamurthi, R.J. Butcher, K. Velmurugan, R. Nandhakumar, Inorg. Chim. Acta, 421 (2014) 80-90.
[16] S. Tardito, L. Marchio, Curr. Med. Chem., 16 (2009) 1325-1348.
[17] C. Marzano, M. Pellei, F. Tisato, C. Santini, Anti-Cancer Agent Me., 9 (2009) 185-211.
[18] C. Santini, M. Pellei, V. Gandin, M. Porchia, F. Tisato, C. Marzano, Chem. Rev., 114 (2014) 815-862.
[19] B.M. Zeglis, V.C. Pierre, J.K. Barton, Chem. Commun., (2007) 4565-4579.
[20] A. Gil, M. Melle-Franco, V. Branchadell, M.J. Calhorda, J. Chem. Theory Comput., 11 (2015) 2714-2728.
[21] H.K. Liu, P.J. Sadler, Accounts Chem. Res., 44 (2011) 349-359.
[22] C. Acilan, B. Cevatemre, Z. Adiguzel, D. Karakas, E. Ulukaya, N. Ribeiro, I. Correia, J.C. Pessoa, Biochim. Biophys. Acta - Gen. Sub., 1861 (2017) 218-234.
[23] M. Fernandez, L. Becco, I. Correia, J. Benitez, O.E. Piro, G.A. Echeverria, A. Medeiros, M. Comini, M.L. Lavaggi, M. Gonzalez, H. Cerecetto, V. Moreno, J.C. Pessoa, B. Garat, D. Gambino, J. Inorg. Biochem., 127 (2013) 150-160.
[24] https://www.molinspiration.com/cgi-bin/properties in 25/10/2019
[25] O.P. Sharma, T.K. Bhat, Food Chem., 113 (2009) 1202-1205.
[26] T. Peters, F. W. Putnam, The Plasma Proteins, Academic Press 1975.
[27] B. Valeur, M.N. Berberan-Santos, Molecular Fluorescence: Principles and Applications, 2nd ed., Wiley, VHC, 2012.

[28] A. Coutinho, M. Prieto, J. Chem. Edu., 70 (1993) 425-428.
[29] J.R. Lakowicz, Principles of Fluorescence Spectroscopy., Kluwer Academic, Plenum Publishers, , New York, 1999.
[30] A. Altomare, G. Cascarano, C. Giacovazzo, A. Guagliardi, J. Appl. Cryst., 26 (1993) 343-350.
[31] M. Ausubel, R. Brent, R.E. Kingston, D.D. Moore, J.G. Seidman, J.A. Smith, and K. Struhl, Current Protocols in Molecular Biology, John Wiley & Sons, New York 1989.
[32] N.C. Santos, M. Prieto, and M.A.R.B.Castanho, Biochim. Biophys. Acta, 1612 (2003) 123-135.
[33] C.V. Kumar, Punzalan, E. H. and Tan, W. B., Tetrahedron, 56 (2000) 7027-7040.
[34] L.J. Bellamy, The infrared spectra of complex molecules, (3rd ed.) ed., Chapman and Hall Ltd., London, 1975.
[35] B. Annaraj, M.A. Neelakantan, Eur. J. Med. Chem., 102 (2015) 1-8.
[36] D. Lin-Vien, N.Colthup, W. Fateley and J. Grasselli, Handbook of Infrared and Raman Characteristic Frequencies of Organic Molecules, Elsevier, 1991.
[37] J. Clayden, N. Greeves and S. Warren, Organic Chemistry, 2nd ed., Oxford University Press, New York, 2012.
[38] A.B.P. Lever, Inorganic Electronic Spectroscopy, Elsevier, New York, 1984.
[39] E.N. Sathyanarayana, Electronic Absorption Spectroscopy and Related Techniques University Press Limited, India, 2001.
[40] A. Rockenbauer, L. Korecz, Appl. Magn. Reson., 10 (1996) 29-43.
[41] U. Sakaguchi, A. W. Addison, J. Chem. Soc. Dalton Trans., 4 (1979) 600-608.
[42] N. Mukherjee, S. Podder, K. Mitra, S. Majumdar, D. Nandi, A.R. Chakravarty, Dalton Trans., 47 (2018) 823-835.
[43] M.B. Pereira, L.A. Fontana, J.D. Siqueira, B.L. Auras, M.P. da Silva, A. Neves, P. Gabriel, H. Terenzi, B.A. Iglesias, D.F. Back, Inorg. Chim. Acta, 469 (2018) 561-575.
[44] M.M. Radanovic, M.V. Rodic, S. Armakovic, S.J. Armakovic, L.S. Vojinovic-Jesic, V.M. Leovac, J. Coord. Chem., 70 (2017) 2870-2887.
[45] P. Domiano, A. Musatti, M. Nardelli, C. Pelizzi, G. Predieri, Transit. Metal Chem., 4 (1979) 351-354.
[46] V.Y. Tyurin, A.A. Moiseeva, D.B. Shpakovsky, E.R. Milaeva, J. Electroanal. Chem., 756 (2015) 212-221.
[47] A. Ricci, G.P. Parpinello, N. Teslic, P.A. Kilmartin, A. Versari, Molecules, 24 (2019).
[48] M. Baranowska, K. Suliborska, W. Chrzanowski, B. Kusznierewicz, J. Namiesnik, A. Bartoszek, Redox Biol., 17 (2018) 355-366.
[49] G. Scalese, I. Correia, J. Benítez, S. Rostán, F. Marques, F. Mendes, A.P. Matos, J. Costa Pessoa, D. Gambino, J. Inorg. Biochem., 166 (2017) 162-172.
[50] J.C. Pessoa, I. Correia, Coord. Chem. Rev., 388 (2019) 227-247.
[51] A.O. Pedersen K.L.D Mensberg, U. Kragh-Hansen, Eur. J. Biochem., 233 (1995) 395-405.
[52] J. Flarakos, Morand, L. K., Vouros, P., Anal. Chem., 77 (2005) 1345-1353.

[53] C.Tan, J. Liu, H. Li, W. Zheng, S. Shi, L. Chen, L. Ji, J. Inorg. Biochem., 102 (2008) 347-358.
[54] W. Bal, J. Christodoulou, P.J. Sadler, A. Tucker, J. Inorg. Biochem. 70 (1998) 33-39
[55] M. Bern, K.M.K. Sand, J. Nilsen, I. Sandlie, J.T. Andersen, J. Control Release, 211 (2015) 144-162.
[56] K. Brodowska, I. Correia, E. Garribba, F. Marques, E. Klewicka, E. Łodyga-Chruscińska, J. C. Pessoa, A. Dzeikala, L. Chruscińskie, J. Inorg. Biochem., 165 (2016) 36-48.
[57] J. Masuoka, J. Hegenauer, B.R. Vandyke, P. Saltman, J. Biol. Chem., 268 (1993) 21533-21537.
[58] Y.Q. Wang, H.-M. Zhang, G.-C. Zhang, W.-H. Tao, S.-H. Tang, J. Lumin., 126 (2007) 211-218.
[59] R.B. Singh, S. Mahanta, A.Bagchi, N. Guchhait, Photochem. Photobiol. Sci., 8 (2009) 101-110.
[60] P.B. Kandagal, S.M.T. Shaikh, D.H. Manjunatha, J. Seetharamappa and B.S. Nagaralli, J. Photochem. Photobiol. A, 189 (2007) 121–127.
[61] Y. Zhang, J.H. Li, Y.S. Ge, X.R. Liu, F.L. Jing, Y. Liu, J. Fluoresc., 21 (2011) 475–485.
[62] C. Dufour, O. Dangles, Biochim. Biophys. Acta, 1721 (2005) 164–173.
[63] J.V. Goodpaster, Vl.L. McGuffin, Appl. Spectrosc., 53 (1999) 1000-1008.
[64] P. Sathyadevi, P. Krishnamoorthy, R.R. Butorac, A.H. Cowley, N.S.P. Bhuvanesh, N. Dharmaraj, Dalton Trans., 40 (2011) 9690-9702.
[65] C.P. Matos, Y. Addis, P. Nunes, S. Barroso, I. Alho, M. Martins, A. P.A. Matos, F. Marques, I. cavaco, J.C. Pessoa, I. Correia, J. Inorg. Biochem., 198 (2019) 110727-110735.
[66] Q.L. Zhang, J.G. Liu, H. Chao, G.Q. Xue, L.N. Ji, J. Inorg. Biochem., 83 (2001) 49-55.
[67] D.S. Raja, Bhuvanesh, N. S. P. and Natarajan, K. , Eur. J. Med. Chem., 47 (2012) 73-85.

Exploring the therapeutic potential of Cu(II)-complexes with ligands derived from pyridoxal

Patrique Nunes: Investigation (synthesis, characterization, biochemical studies), original draft preparation; **Fernanda Marques:** Investigation (cytotoxicity); **Isabel Cavaco:** Methodology: writing-reviewing; **João Costa Pessoa**; Writing-reviewing, formal analysis**; Isabel Correia:** Conceptualization, methodology, writing-reviewing.

Declaration of interests

☐☑ The authors declare that they have no known competing financial interests or personal relationships that could have appeared to influence the work reported in this paper.

☐The authors declare the following financial interests/personal relationships which may be considered as potential competing interests:

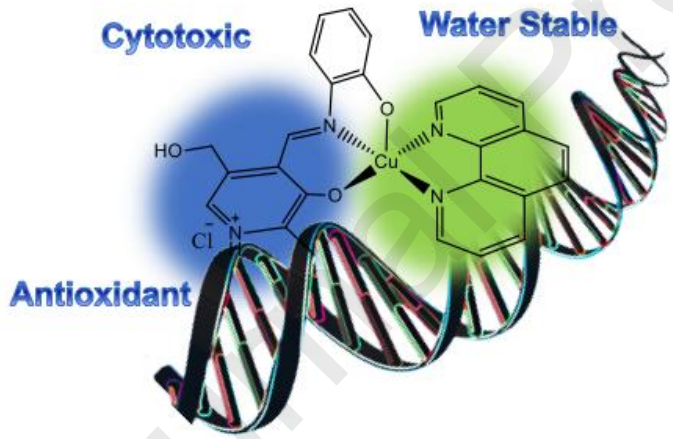

Cu(II) complexes containing pyridoxal Schiff bases and 1,10-phenanthroline show cytotoxicity against tumor cells related with their ability to bind DNA by intercalation.

- New Schiff base complexes, [Cu(L)(X)], derived from pyridoxal are characterized.
- One Schiff base shows very high radical scavenging activity (dpph assay).
- IC_{50} values in the μM range are found against breast and ovarian cancer cells.
- Ternary complexes containing 1,10-phenanthroline show the highest cytotoxicity.
- Ternary complexes show *in vitro* ability to target DNA through intercalation.